Ancient TL

www.ancienttl.org · ISSN: 2693-0935

Issue 40(2) - December 2022
https://doi.org/10.26034/la.atl.v40.i2

ISSN 2693-0935

Ancient TL

A periodical devoted to Luminescence and ESR dating

Department of Physics, East Carolina University, 1000 East 5th Street, Greenville, NC 27858, USA
http://ancienttl.org

December 2022, Volume 40 No.2

Ancient TL

Started by the late David Zimmerman in 1977

Ancient TL

Luminescence Dating of Quartz: A MATLAB-Based Program for computation of SAR paleodoses using natural sensitivity correction (NCF)

Rahul Kumar Kaushal[1*], Naveen Chauhan[1], Ashok K. Singhvi[1]

[1] AMOPH Division, Physical Research Laboratory, Navarangpura, Ahmedabad 380009, India
*Corresponding Author: rahulkiitgn@gmail.com

Received: November 18, 2022; in final form: December 8, 2022

Abstract

This study presents a MATLAB based program to implement the natural sensitivity correction (NCF) for the assessment of single aliquot regeneration based paleodoses (Singhvi et al., 2011; Chauhan & Singhvi, 2019). Several software packages /spreadsheets are in use to calculate the SAR paleodoses (D_es) but do not offer the facility for such a correction. The user-friendly program presented here, computes NCF-SAR paleodoses (D_es) and includes the errors in the measured NCF values. Monte-Carlo simulation was used to propagate the uncertainties in the paleodoses from the NCF and uncertainties in curve fitting parameters.

Keywords: NCF-SAR, paleodose, MATLAB, Monte-Carlo simulation

1. Introduction

In luminescence dating, the single aliquot regeneration protocol (SAR) is routinely used to estimate the paleodoses (Murray & Wintle, 2000). An addition to this protocol, the natural sensitivity correction (NCF), was suggested by Singhvi et al. (2011) to account for sensitivity changes that occur during the preheat and readout of natural OSL. When ignored, this sensitivity change leads to systematic offsets in paleodoses (Figure 1) and results in higher dispersion in D_e values, (Singhvi et al., 2011; Chauhan et al., 2015; Chauhan & Singhvi, 2019). Use of NCF also enables handling of samples when the natural OSL intensity is higher than the luminescence intensity at the saturation dose of the regenerated curve for SAR-corrected measurements.

NCF is measured as the ratio of the 110 °C TL peaks before and after the measurement of natural OSL. Tables 1 and 2 provide the measurement schedule for the conventional and the NCF-SAR protocols. Though necessary, available softwares do not include any provision to include the NCF. We present here a user-friendly MATLAB based program for inclusion of NCF in the calculation process. The uncertainties in the paleodoses of NCF are propagated using the Monte Carlo method (MCM) (Figure 2).

This program requires input data on an Excel spreadsheet in a specified format. It then carries out multiple MATLAB functions to calculate the NCF-SAR paleo-doses. It enables analysis of multiple aliquots or samples in a single operation by uploading appropriate files, one for each sample. Appendix A and the supplementary file provide relevant details for the use of the program for computation. The output is provided as an Excel spreadsheet.

Table 1: Generalized single-aliquot regeneration (SAR) protocol by Murray & Wintle (2000)

Steps	Treatment	Remarks
1	Give dose D_i	-
2	Pre-heat (160 – 300 °C,10s)	-
3	OSL (40s, at 125 °C)	L_i
4	Give test Dose	-
5	Preheat (160 – 300 °C)	-
6	OSL (40s, at 125 °C)	T_i
7	Return to step 1	

For the natural sample, i=0, and D_0 = 0 Gy; L_i and T_i are derived from the stimulation curve, typically the first 1 – 10 s of initial OSL signal, minus a background estimated from the last part of the stimulation curve.

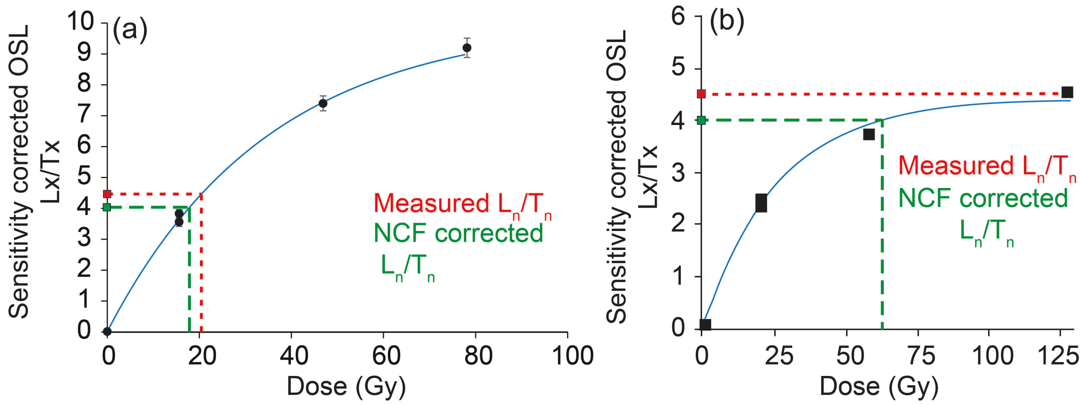

Figure 1: Response curve of sensitivity corrected OSL (L_x/T_x ratio) vs. dose (i.e. growth curve) of quartz samples from desert dunes to show sensitivity change during natural measurement. NCF corrects for these sensitivity changes even in the saturation range. (Data in Figure b from Chauhan et al. 2015).

Steps	Treatment	Remarks
1	Natural Sample	Pure quartz on SS discs
2	Dose for NCF	Small dose added to natural sample
3	*TL to 200 °C at 2 °C/s for 10 s	TL_1
4	Preheat (160 – 300 °C) 10 s	SAR preheat
5	OSL** at 125 °C for 40 s	OSL (L_n)
6	Cut heat (200 °C)	To remove charge from possible phototransfer, if any and photo-transfer
7	Test Dose	Small dose added to sample
8	TL to 220 °C at 2 °C/s for 10 s	TL_2
9	OSL at 125 °C for 40 s	OSL (T_n)
10	Regeneration dose (R_1, R_2, R_3, 0, R_1)	
*TL-integration peak ± 15 °C or peak ± FWHM ** If sample contains feldspar as inclusion, use of IR bleaching at 50 °C for 100 s is recommended before every OSL measurements to subdue the contribution of feldspar.		

Table 2: The NCF-SAR method for calculating the natural correction factor (TL_2/TL_1) to correct sensitivity change occurring during natural OSL measurement. The remarks of each step are given for clarity.

2. Calculation Procedure

The following sequence is used to calculate NCF corrected doses (Figure 2).

1. The NCF is computed as

$$NCF = \frac{TL_1(IntegratedCounts)}{TL_2(IntegratedCounts)} \tag{1}$$

   TL_1 is integrated TL counts for 110 °C before preheat and natural OSL measurement and TL_2 is integrated photon counts after readout of natural OSL (Table 1, Singhvi et al. 2011). A typical integration range could either be peak ± 15 °C or peak ± FWHM, with measurements at a heating rate of 2 °C/s.

2. These are used to correct individual normalized natural OSL

$$\left(\frac{L_n}{T_n}\right)_{corrected} = \frac{1}{NCF} \times \frac{L_n}{T_n} \tag{2}$$

   The error in this is propagated as for a ratio. The NCF corrected (L_n/T_n) ratio and its error are used to generate a Gaussian probability density function (pdf) from which values can be picked randomly.

3. Parameters (*a, b, c*) and their associated errors from the fitting of the typically exponential growth curve

$$Y = a\left(1 - e^{-\frac{x+c}{b}}\right) \tag{3}$$

   are then picked up from the instrument software and a Gaussian probability density function for each is generated such that the standard deviation (1-sigma error) represents the width of the distribution. From these, random data points are generated and for each set of such data points, a corresponding D_e is computed. Typically, for each parameter, 10,000 stochastic values are generated using Monte-Carlo simulations. The random numbers are created through the 'rand' function in MATLAB which uses the Ziggurat random normal generator based on Marsaglia (1968).

4. The mean and standard deviation of the resulting distribution give the D_e value and its error for each aliquot respectively whether they are single or multiple grains.

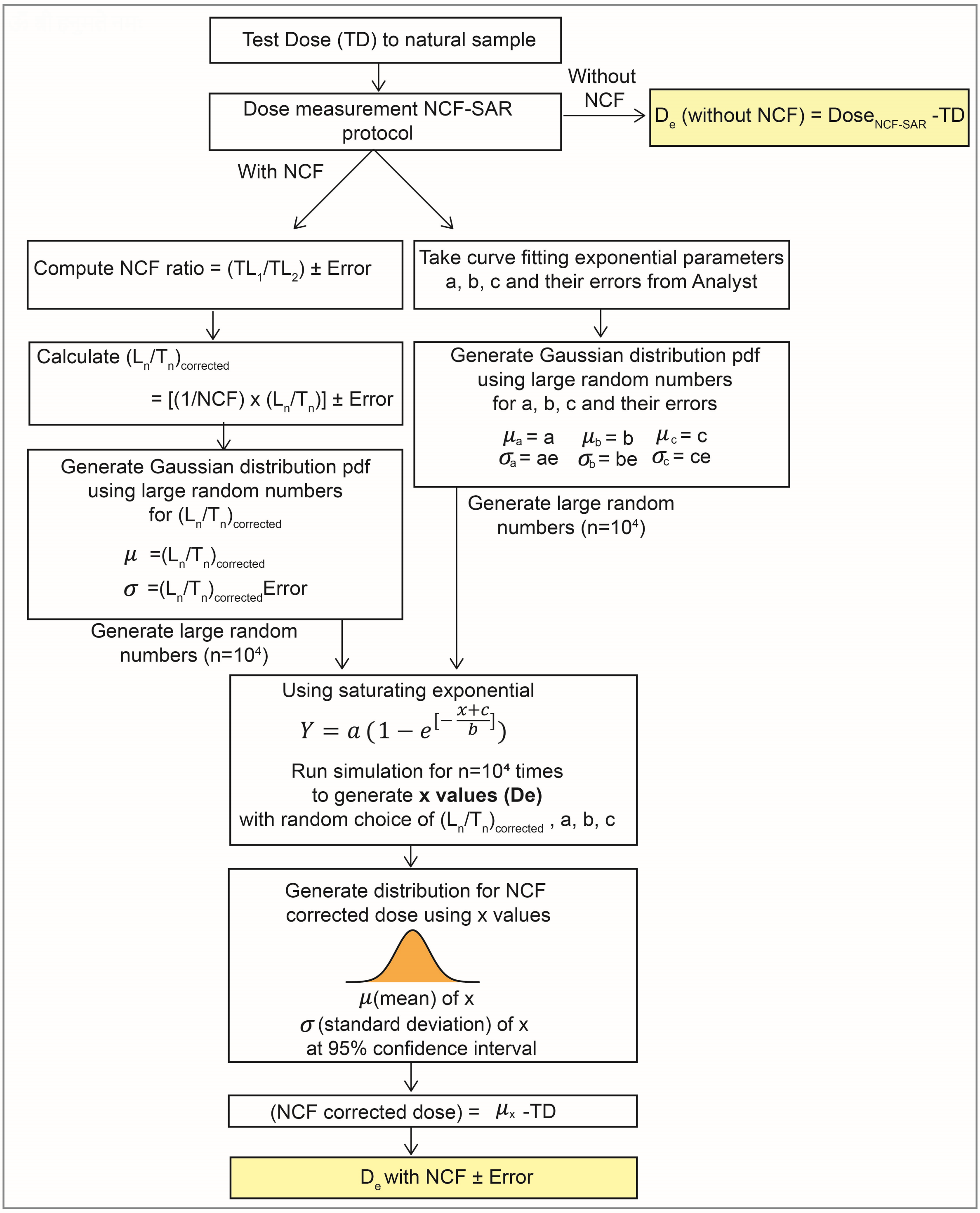

Figure 2: Steps for the calculation of the NCF corrected dose

3. Results and Discussion

Figure 3 shows typical results for the statistical distribution of NCF corrected dose values from the above computations. The histogram shows D_e values for each of 10,000 computations. The number 10,000 was determined based on Figure 4 when D_e and its error stabilized. The mean or central value of the paleodose D_e and its standard deviation (1-sigma uncertainty) was obtained from analysis of the resulting distribution of D_e values of single aliquots (Figure 3). This same procedure was carried out for the remaining aliquots to obtain their mean D_e value along with its error. Finally, data for all of the aliquots with their NCF corrected D_e and their errors were collated to create a histogram (Figure 5). A comparison of NCF-corrected D_e with NCF-uncorrected D_e is given in Table 3 and Figure 5. The NCF ratio for sample TNLW-3 ranges from 0.81 to 1.2 indicating that an aliquot-specific NCF value is needed.

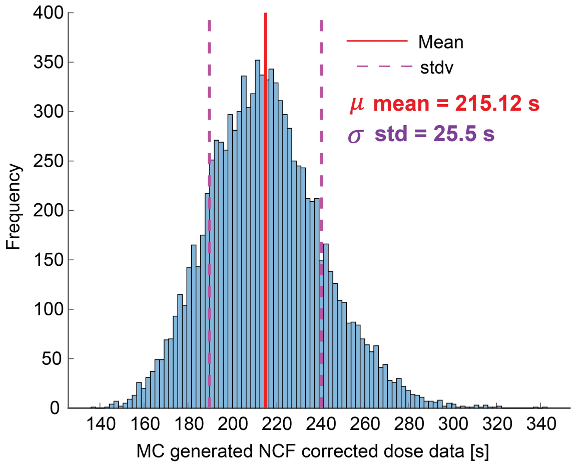

Figure 3: Histogram of Sample TNLW-3 (for disc-5) showing result of the Monte-Carlo simulation to obtain D_e distribution and its standard deviation.

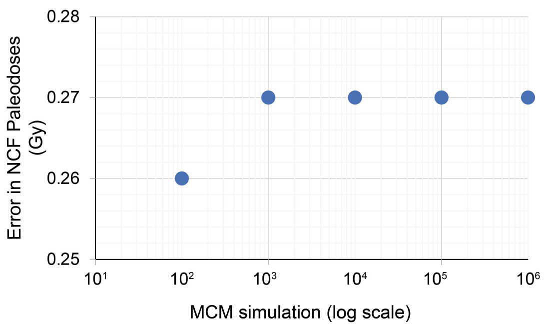

Figure 4: Error in NCF paleodoses stabilises with increasing number of MCM simulations.

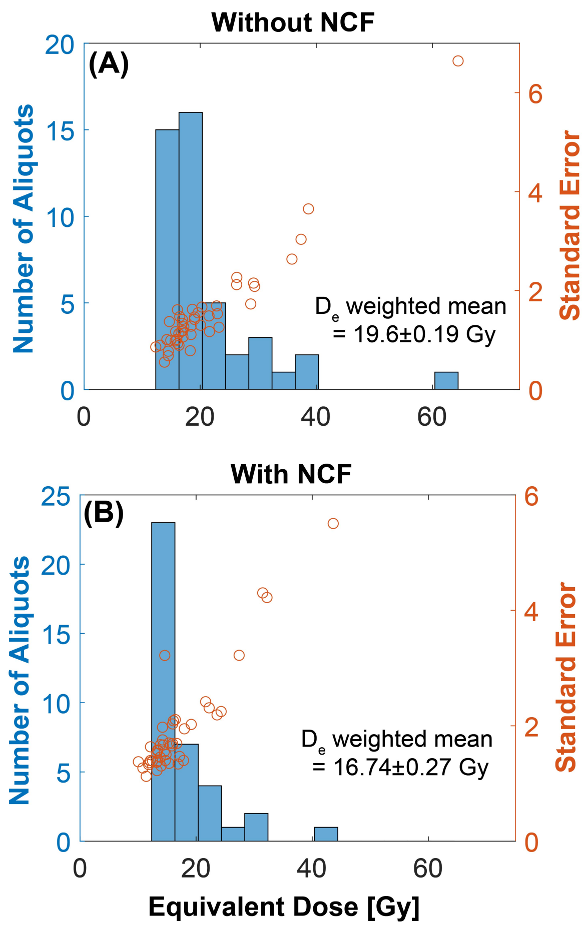

Figure 5: Comparison of dose distributions obtained with and without NCF-SAR correction. Reduced scatter in the MCM-derived standard error of D_e is also noticeable as the NCF correction is applied.

4. Conclusion and Summary

A user-friendly program for applying the NCF-SAR protocol is proposed that uses Monte-Carlo simulations and errors integration in NCF in the final corrected paleodose. On applying an MCM approach for error propagation minor changes in NCF corrected paleo-doses and in their error are seen. The NCF-SAR procedure results in lower dispersion in paleodoses and significantly lower paleodoses.

Acknowledgements

AKS thanks DST-SERB, India for financial support through a DST-YOSCP grant and Dr. Sanjay Singh Negi and Dr. Ramendra Sahoo for testing the MCM method in MATLAB. We thank Prof. Michel Lamothe for his helpful and constructive review. Dr. Regina DeWitt kindly processed the manuscript within a short time.

Sample	Depth (m)	D_e (Gy)		%-Change in D_e
		Without NCF	With NCF	
TNLW-1	0.5	3.6 ± 0.1	3.0 ± 0.1	16
TNLW-2	1.5	10.1 ± 0.3	8.9 ± 0.3	11
TNLW-3	2.36	19.6 ± 0.2	16.5 ± 0.3	17
TNLW-5	4.26	20.9 ± 0.2	17.2 ± 0.3	17
TNLW-6	5.11	21.3 ± 0.2	19.9 ± 0.2	7

Table 3: Variations in paleodoses (D_e) on applying the NCF correction factor and their percent-change in samples from the Thar Desert.

Appendix: Procedure for input data format and executing NCF-SAR MATLAB program

1. To run these functions, no programming skills or advanced MATLAB capability are needed and the following steps will help computations. Open Relevant Analyst file → Go to top menu bar in Analyst → Records → Unselect All → Every Record

2. Records tab → Select All → Records of type → Select records of OSL → Click on SAR button → A Single Aliquot Analysis: window will open.

3. Choose Integration Limits for Signal and Background → Go to Curve Fitting → Select exponential fit → Set acceptance Criteria: - Recycling ratio limit (%) =10; Max. test dose error (%) = 10; Max. paleodose error (%) = 10; Max. Recuperation (%) = 5; Tick () on Incorporate error on curve fitting.

4. Now Go to Function tab → Analyse All Grains by accounting all acceptance Criteria

5. Go to Summary Data tab → Select all aliquots that have passed criteria and gave D_e values (use Shift + Right arrow on keyboard) → Right click on selected area → Copy data to clipboard with headers → Paste it to any *.txt file or Excel file

6. From this data, select only following columns which will be used for NCF analysis and copy them in an Excel sheet- (1) Filename (2) Disc (3) ED (4) ED_err (5) L_n/T_n (6) L_n/T_n_err (7) Param1 (8) Error1 (9) Param2 (10) Error2 (11) Param3 (12) Error3

7. Close this Single Aliquot Analysis window

8. To extract data for the TL_1 and TL_2 counts- follow step-1 again and make sure Selected column show 'False'.

9. From Display information menu → Click on Integral1 to integrate counts around the peak ± 15 °C region. (For example: lower and upper integration limit was 85 °C and 105 °C respectively for the TNLW-3 sample)

10. Repeat step-9 to obtain TL_2 Integral counts.

11. To export TL_1 and TL_2 integrated counts; Carefully choose Lumin. Type and Run Number as per Table-2 NCF-SAR protocol steps. (For example: Lumin. Type = TL And Run Number = 2 → will select TL_1 integrated counts; Lumin. Type = TL And Run Number = 7 → will select TL_2 integrated counts)

12. Once all necessary data has been extracted, we can arrange the step-6 columns and TL integrated counts in the sequence with headers shown in Table A1

    Note: The fitting parameters (*a, b, and c*) for the saturating exponential are saved as Param1, Param2 and Param3 along with their errors.

    It is to note that the machine dose rate (Gy/min) will be used to calculate the final paleodose (D_e) in Gy by using the actual dose rate calculated at the time of experiment. The irradiation raw data obtained from analyst is in seconds. It is kept in the mentioned units so as to minimize data processing by the user. Date formatting should be as D-M-YYYY.

13. To run ***NCF-SAR*** MATLAB program, MATLAB function files are best kept in the same folder or add them to MATLB path. Then user needs to open a MATLAB command window and recall the function by typing command ***load_NCFSAR_data*** and run the program by clicking on Run button or pressing F5 in MATLAB upper panel. This will open a new menu window and navigate to the current folder where all the sample excel files are placed. User can select any file and follow instructions visible on the MTALB command window (Fig. A1). If any user has multiple files to process, then name them as ***sample name_***. This program takes input file as both .csv or excel file format with a single spread sheet. (The program to run with or without MCM calculation is based on user choice). On execution, the NCF-SAR program provides the sensitivity corrected paleo dose estimates in a separate excel file (***sample name_result_NCF_SAR***) along with a dose distribution plot. These are automatically saved in the ***'result'*** folder. The NCF corrected dose data can be analysed through various platform (e.g., R or DRAC calculator) to calculate final age.

The NCF-SAR MATLAB program, together with steps

1	2	3	4	5	6	7	8	9
File name	date	Disc position	ED	ED_ err	TL_1	TL_2	L_n/T_n	L_n/T_n_err

10	11	12	13	14	15	16	17	18	19
a	a_err	b	b_err	c	c_err	NCF Test dose	Machine Dose Rate (Gy/min)	Machine calibration date (D-M-YYYY)	Experiment date (D-M-YYYY)

Table A1: Arrangement of data (see step 12 of the Appendix)

and the example data presented in this publication as input for the code, can be downloaded from the Ancient TL webpage. It is also available from Github, an open access open-source platform website (https://github.com/Rahulkaushal009/NCFSAR-tool).

References

Chauhan, N. and Singhvi, A. K. *Changes in the optically stimulated luminescence (OSL) sensitivity of single grains of quartz during the measurement of natural OSL: Implications for the reliability of optical ages*. Quaternary Geochronology, 53: 101004, 2019.

Chauhan, N., Choi, J. H., Kim, J. Y., and Lee, G. *Application of newly developed NCFSAR protocol to Quaternary sediments from Suncheon and Jeongok, South Korea*. Geosciences Journal, 19: 407–413, 2015.

Marsaglia, G. *Random numbers fall mainly in the planes*. Proceedings of the National Academy of Sciences, 61: 25–28, 1968.

Murray, A. S. and Wintle, A. G. *Luminescence dating of quartz using an improved single-aliquot regenerative-dose protocol*. Radiation Measurements, 32: 57–73, 2000.

Singhvi, A., Stokes, S., Chauhan, N., Nagar, Y., and Jaiswal, M. *Changes in natural OSL sensitivity during single aliquot regeneration procedure and their implications for paleo dose determination*. Geochronometria, 38: 231–241, 2011.

Reviewer

Michel Lamothe

Reviewer comment:

A useful and timely manuscript as the NCF correction needs to be easily computable in cases where such quartz OSL sensitivity issues are significant.

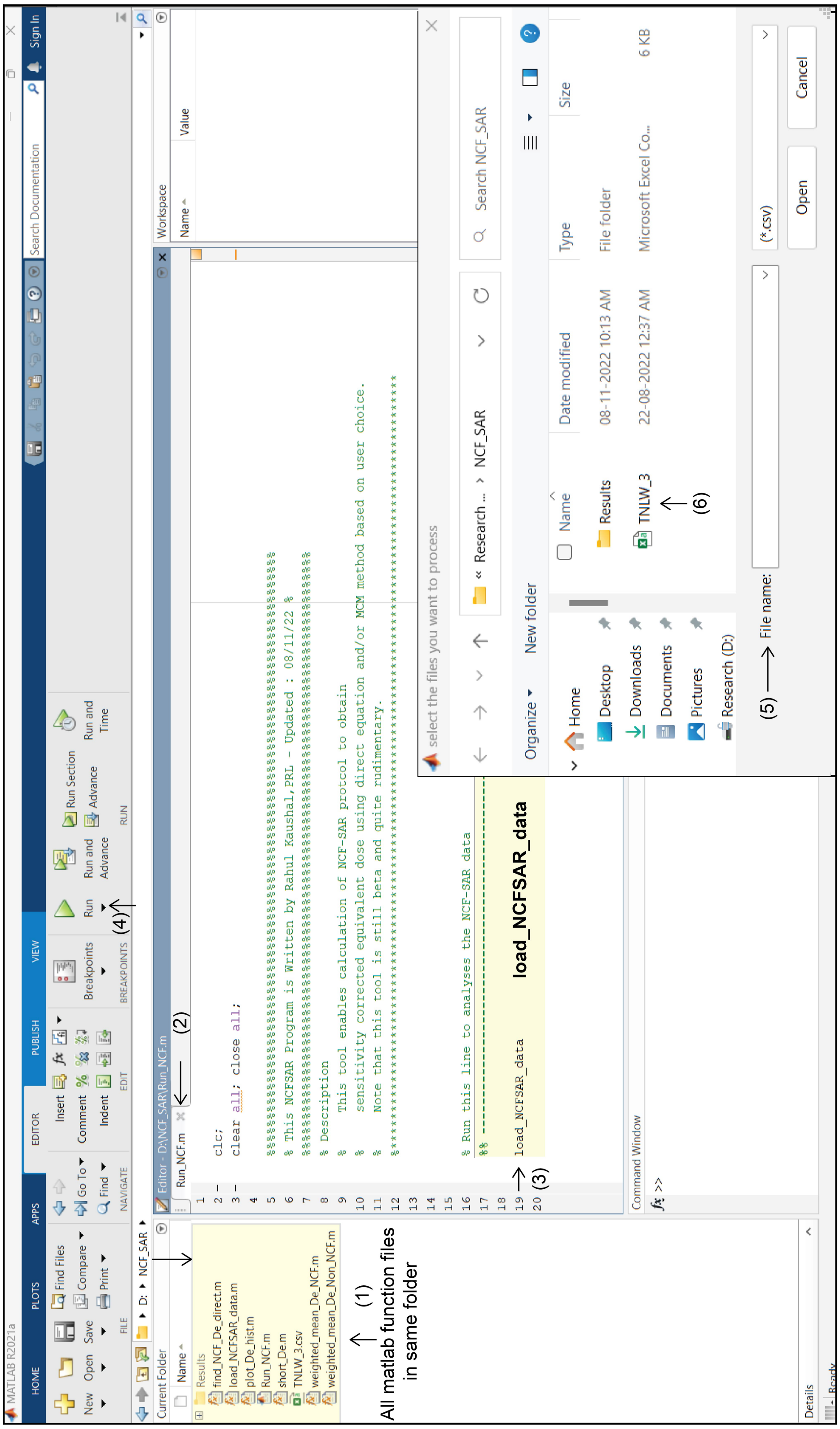

Figure A1: Steps to run the NCFSAR program and select the appropriate file

Ancient TL

Methods Note: The extended minimum extraction technique: an update on sampling protocols

Amber G. E. Hood[1]*

[1] Department of Geology, Lund University, Sweden
*Corresponding Author: amber.hood@geol.lu.se

Received: November 2, 2022; in final form: December 19, 2022

Abstract

This paper communicates an update to the minimum extraction technique (MET) sampling protocol (a means by which to extract and subsequently measure a minute sample from museum objects for luminescence dating), designated the extended MET protocol. The new protocol facilitates a sample yield of approximately double that of the original MET protocol without altering the outward appearance of the sampling mark on archaeological materials. This development is useful when working with museum materials where the visual integrity of artefacts often takes precedence over access to sampling for luminescence analysis.

Keywords: minimum extraction technique, ceramics, museum artefacts, optically stimulated luminescence

Figure 1: A (top): 1.5 mm diamond disc burr drill bit; B (middle): 2 mm diamond ball burr drill bit; C (bottom): 1.5 mm diamond core drill bit; all three drill bits are used in the extended MET sampling protocol.

1. Introduction

The minimum extraction technique (MET) sampling protocol was first presented by Hood & Schwenninger (2015) as a technique which enabled sampling for absolute optically stimulated luminescence (OSL) dating while at the same time minimising the quantity of sample required for extraction from ceramic (and similar artefacts such as mud seals) housed in museum collections. While it can of course be argued that OSL dating of non-museum ceramics (i.e. from recent excavations) can yield more robust and routine data, working with museum materials is often a necessity, e.g. when access to OSL dating is not possible in certain regions or local laws prevent analysis of recently excavated material.

2. The extended MET drilling method

Initially, MET sampling saw the removal of a sample from an artefact measuring *c.*2 mm x 4mm in volume using a hand drill. The first 2 mm x 2 mm of removed material was recovered using a 2 mm diamond ball burr drill bit (Figure 1B) and was used for internal dose rate ($\dot{D}_{int}$) measurement. The subsequent (i.e. below) 2 mm x 2 mm sample was then removed using a 1.5 mm diamond core drill bit (Figure 1C) and it was

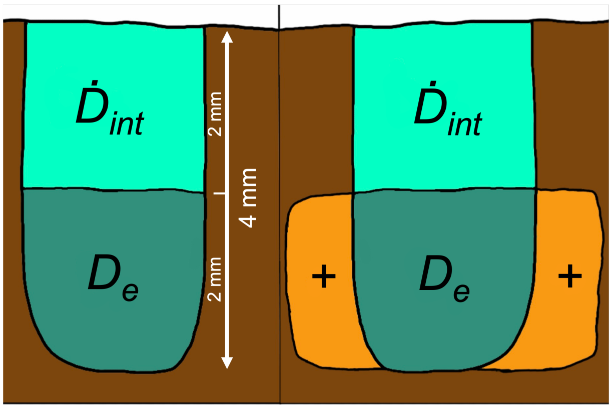

Figure 2: A schematic of original (left) and new (right) MET sampling; the '+' illustrates the laterally removed additional sample that improves MET "sample" yield.

this sample that was previously used for equivalent dose (D_e) measurement.

In the extended MET protocol, the removal of the $\dot{D}_{int}$ sample remains unchanged. The removal of the D_e sample also remains the same at first, however it is extended by an additional step. This new, final step uses a 1.5 mm diamond disc burr drill bit (Figure 1A) to carve out additional material laterally around the initial D_e sample; this lateral drilling is achieved by moving the flat drilling head both circularly and vertically between 2 mm and 4 mm in depth below the surface of the vessel. Because only the smooth shaft of the drill bit is at the surface of the vessel, no additional erosion of the top 2 mm occurs. The differences between the two methods are presented schematically in Figure 2. Figure 2 also illustrates that the additional material is suitable for D_e measurement as it comes from 2 mm below the surface of the vessel and thus avoids potential sample contamination from either light or external beta particles (cf. Feathers 2009).

3. Results

This updated, extended MET sampling method yields a significantly increased sample size, resulting in more material being available for D_e measurement without affecting the visible mark of the surface of the artefact where the sample is taken (Figure 3). Table 1 illustrates how for a test sherd, the increase in yield from MET sampling to extended MET sampling across 10 samples was just over 100%.

4. Discussion

As the density, and thus mass, of a ceramic is highly variable from vessel to vessel (or sherd to sherd), it is not possible to quantify the yield increase according to mass in absolute terms for all potential samples. As such, extended MET protocol samples carried out on other artefacts may produce different masses to those seen in Table 1, which are specific to the sherd used to demonstrate the inceased sample yield

Figure 3: A ceramic sherd (sub-sambled from MM 34209; details available here) from the Medelhavsmuseet (Museum of Mediterranean and Near Eastern Antiquities), Stockholm, displaying 10 individual sample holes on its surface; holes 1 – 5 result from the extended MET protocol, and holes 6 – 10 are those made by the original MET protocol. All visible surface holes remain at 2 mm in diameter.

resulting from the extended MET protocol presented here.

Volumetrically the increase is also difficult to quantify in absolute terms as we are not able to see beneath the surface of the sherd, but it is expected that, as with the increase in mass, the increase in volume is approximately double, as illustrated in Figure 2. It should also be noted that both the MET and extended MET sampling protocols are carried out by hand, often in make-shift laboratory conditions in museums where sampling takes place. As such, the visual presented in Figure 2 is a guide only and natural variation owing to the nature of hand drilling may see the cavity made by extended MET drilling go slightly wider and/or deeper than in Figure 2. However, it will not change the visual appearance of the sampling location on the surface of the vessel.

While each individual ceramic sherd is unique (and thus

	MET	Extended MET
	8 mg	16 mg
	9 mg	17 mg
	10 mg	19 mg
	8 mg	19 mg
	7 mg	19 mg
	7 mg	17 mg
	8 mg	20 mg
	6 mg	13 mg
	5 mg	12 mg
	7 mg	19 mg
Mean	7.5 mg	17.1 mg
Std dev	1.43 mg	2.73 mg

Table 1: Difference in sample mass yield between the MET and the Extended MET sampling protocols. NB variations in sample weight are likely resulting from the heterogeneity of the ceramic fabric, coupled with voids within the ceramic matrix, caused, e.g., by organic inclusions that have been burnt away. A portable digital scale, reading to three decimal places was used to weigh each sample.

each sampling action is unique) it has been my experience that the new extended MET protocol has an identical visible surface footprint to the original MET protocol, because the surface above the expanded sample remains stable. I therefore expect that this new technique is suitable for both intact and fragmentary objects. To date, this extended MET protocol (and indeed the MET protocol before it) has not caused structural issues for sampled objects and can be, in general, considered a suitable sampling protocol for museum ceramics. However, caution should always be exercised by the luminescence practitioner when dealing with new, unfamiliar material as the uniqueness of each individual piece could render destructive sampling difficult for certain artefacts, particularly if their matrix is of a particularly friable nature.

An additional benefit of the extended MET protocol is that is also permits sampling with increased yield of ceramics with thinner profiles. In general, if working with complete vessels, the ideal sample location is the base of the vessel (as it is usually both the thickest part of the vessel, and the most sturdy and the most inconspicious place to sample). However, to ensure that the required 2 mm of surface material remains in place to ensure no contamination from light or beta particles, an artefact thickness of at least 6 mm was required for the original MET protocol. This depth was necessary to allow 2 mm to be remaining between the sample location and the interior or back surface even after the 4mm sample was removed from the exterior surface (2 mm removed for $\dot{D}_{int}$ determination, plus the 2 mm sample for D_e measurement). As such, a 6 mm vessel profile was required for successful MET samping. A profile width of 5 mm could be worked with if necessary, however with the original MET sampling, this meant a significantly reduced D_e sample could be taken. However with the extended MET protocol, even when working with a thinner ceramic profile of 5 mm, it is in theory possible to achieve a D_e sample yield which is approximately equal to the sample volume achievable with the standard MET protocol, as it is possible to remove additional sample laterally within the central 1 mm of suitable sample at the middle of the vessel wall.

5. Conclusion

This paper has presented an update to MET sampling, termed the extended MET, which sees an increase of $\sim$100% yield for the D_e sample compared to the sample yield that the original MET sampling protocol delivered. This is a significant improvement in the sample sizes that can be taken from museum objects whilst still ensuring that a minimum amount of damage is caused and that the aesthetic integrity of the artefact is upheld. The extended MET protocol is thus recommended for use by those luminescence practitioners who work with museum objects.

Acknowledgments

Thanks go to the Museum of Mediterranean and Near Eastern Antiquities (Medelhavsmuseet), Stockholm, Sweden, especially Sofia Häggman, Mia Broné and Adam Norberg, for providing the ceramic sherd used in this research. The funding for this work was provided by the German Research Foundation, Germany (Deutsche Forschungsgemeinschaft) and the Royal Physiographic Society of Lund (Kungliga Fysiografiska Sällskapet i Lund), Sweden. Thanks are also extended to Helena Alexanderson and Edmund Highcock for providing comments on the manuscript.

References

Feathers, J. K. *Problems of ceramic chronology in the Southeast: does shell-tempered pottery appear earlier than we think?* American Antiquity, 74(1): 113–142, 2009.

Hood, A. and Schwenninger, J.-L. *The Minimum Extraction Technique: A New Sampling Methodology for Optically Stimulated Luminescence Dating of Museum Ceramics.* Quaternary Geochronology, 30: 381–385, 2015.

Reviewer

Jim Feathers

Thesis Abstracts

Index

Harriet Cornachione

Holocene Chronostratigraphy of Dune Fields in Southern Utah: Geomorphic Record of Past Aridity in the Central Colorado Plateau

August 2022
Utah State University, Logan, United States
Degree: Ph.D.
Supervisor: Dr. Tammy Rittenour

The Southwestern United States has a semi-arid climate and is currently in a hydrologic drought that exceeds in magnitude and duration any period of drought in at least five centuries. Evidence of past migrations by Indigenous communities and the appearance/rise of other cultural adaptations in the archaeological record during previous episodes of aridity provide warning of similar disruption in modern times. This is especially of concern given that climate models predict conditions of aridity in this region will be exacerbated in the future due to anthropogenic climate change. Better understanding of the natural variability of hydroclimate will inform both adaptive strategies for future climate change and improved climate forecasts. While instrumental records only span the last <100 years, paleoclimate archives (i.e., tree-rings, sediment deposits) can provide longer duration records that provide a baseline for the frequency and magnitude of past aridity.

This dissertation investigates two dune fields on the central Colorado Plateau in southern Utah. A chronostratigraphic record of eolian activity is developed to determine periods of dune-field activation as an indicator of hydroclimate conditions during the Holocene. Methods and datasets used in this research include geomorphic mapping, descriptions of stratigraphy and sedimentology, optically stimulated luminescence and radiocarbon dating, geochemical analysis of sediments and analysis of regional wind data.

The Kanab dune field in southwestern Utah is a largely stable dune field with parabolic dunes of 2 – 15 m in height. The dune field is oriented roughly west to east. Chronostratigraphic records were used to identify five periods of dune-field wide eolian activity: K0 (~ 9.2 – 7.8 ka), K1 (~ 6.8 – 5.6 ka), K2 (~ 4.4 – 3.3 ka), K3 (~ 2.2 – 1.2 ka) and K4 (~ 0.7 – 0.4 ka). Activity events occur at millennial intervals, and coincide with Bond events and other global climate records, suggesting a climate driver. The San Rafael dune field in east central Utah contains thin (2 – 6 m tall), east-northeast trending dune forms, partially stabilized with soil biocrusts and xeriphytic shrubs, with sections of currently active parabolic dunes and smaller barchan dunes and dune fields. Seven episodes of eolian activity were determined from chronostratigraphy in the dune field: SR0 (~ 17 – 16.2 ka), SR1 (~ 12.4 – 11.2 ka), SR2 (~ 9.7 – 7.4 ka), SR3 (~ 4.7 ka), SR4 (~ 3.4 – 2.5 ka), SR5 (~ 2.0 – 1.6 ka) and SR6 (1.1 – 0.4 ka). Thin deposits and discontinuities in the record suggest an erosion-dominant landscape. Results from both dune field indicate three periods of coeval dune activation in the two dune fields at ~ 9.5 – 7.5 ka, ~ 2 – 1.5 ka, and ~ 1 – 0.5 ka. These are interpreted to record periods of regional aridity. Records of mobile dune activity from other sites across the Colorado Plateau suggest at least three and as many as five periods of regional dune activity interpreted to be related to regional aridity.

Analysis of weather station data indicate that modern wind regimes are consistent with dune field orientation, suggesting they are a useful analog for Holocene winds. Analysis of dune sediment geochemistry using K/Rb-K/Ba suggests that the sediment source material did not change between periods of dune activation. This result supports interpretation of a climate driver for dune field (re) activation events and not changes in sediment supply.

A PDF of this thesis can be downloaded from: https://doi.org/10.26076/606f-c35f

Michael Hein

Beyond the trenches – A landscape-oriented chronostratigraphic approach to MIS 5 Middle Paleolithic open-air sites on the European Plain. Case studies from Lichtenberg and Khotylevo I

November 2021
Max Planck Institute for Evolutionary Anthropology (MPI EVA), Department of Human Evolution, Leipzig, Germany
Degree: Ph.D.
Supervisors: Prof. Jean-Jacques Hublin (MPI EVA); Dr. Tobias Lauer (MPI EVA); Dr. habil. Hans von Suchodoletz (Leipzig University)

The research presented in this thesis aims to establish robust chronostratigraphic frameworks for Late Pleistocene Neanderthal open-air sites on the European Plain, because

well-dated occupations are largely missing so far beyond the range of radiocarbon. It is argued that a firm chronological and stratigraphic foundation is the prerequisite for understanding Neanderthal behavior and its potential synchronization with environmental or climatic events. Only that way, behavioral traits can be inspected in terms of adaption to corresponding developments and changes. This is trying to be illustrated by conducting case studies at Khotylevo I, Western Russia and Lichtenberg, Northern Germany at opposite ends of the European Plain. Very deliberately, the surroundings of these sites were included into the consideration. These can provide insightful background information, which help to better decipher site formation processes and may also elucidate Neanderthal habitat preferences. The two study sites share many similarities, concerning their northern locations, the stratigraphic potential of their embedding sediment sequences and their artifact assemblages, dominated by *Keilmessers*. The latter are asymmetrical, bifacial backed knives, usually made from flint and they represent the type tools for the late Middle Paleolithic period in Central and Western Europe. While for both sites, previous chronological data rather support an assignment to MIS 3, the characteristics of their deposits also made an earlier occupation in MIS 5a seem possible. This ambiguity was to be resolved using geomorphological surveys, pIRIR290 luminescence dating on potassium feldspar (ca. 30 samples) and sediment analyses, the latter also including palynology for additional environmental context. The chronostratigraphic results led to a revision of the timing for the occupations at the two sites: In Khotylevo I it happened during MIS 5a and in Lichtenberg at the MIS 5a/4 transition. The new ages are consistent with the stratigraphic and paleoenvironmental findings and are therefore considered robust and reliable. They provide evidence for an emergence of the *Keilmessergruppen* before the onset of the first glacial maximum in MIS 4, which had been a matter of debate so far. The MIS 5a/4 occupation in Lichtenberg further demonstrates Neanderthal capability to cope with severely cold conditions that could be reconstructed for that phase on site.

The landscape-oriented approach of the investigations directly resulted in the discovery of two hitherto unknown occupations at the site of Lichtenberg. The first one could be allocated to the Mid-Eemian Interglacial (Pollen Zone E IVb/V), the second one was dated and palynologically assigned to the late Brörup Interstadial (ca. 90 ka, Pollen Zone WE IIb). Since the artifacts from these two fully-forested intervals differ from the later *Keilmesser*-dominated artifact assemblages considering shape, size and tool variability, it is proposed that changing environments co-determined the lithic technology.

Chronostratigraphic achievements also include i) the first comprehensive chronology for the widespread 2nd fluvial terrace (MIS 5b to MIS 3) on the Russian Plain, ii) a first numerical age for the termination of the Brörup Interstadial (ca. 90 ka) in its type region, and iii) the first detection of climatic fluctuations during the MIS 5a/4 transition on the European Plain (correlated with Greenland Interstadials GI-20 and GI-19). These findings will help to better contextualize contemporaneous archaeological sites in the wider region.

A PDF of this thesis and the three included journal articles can be downloaded from: `https://www.researchgate.net/profile/Michael-Hein-8`

April I. Phinney

Investigating the Use of Quartz Luminescence and Rock-Color Alteration to Characterize Wildfire Exposure; Applied to the 2020 Mangum Fire, Kaibab Plateau, Arizona

December 2022

Utah State University, Logan, United States

Degree: M.Sc.
Supervisor: Tammy Rittenour

Wildfires appear to be increasing in size, severity, and frequency. Land managers need information on past wildfire behaviour to make effective and adaptive land management plans. However, there are only a few techniques and data sources that provide information on past fire heating. This study aims to provide new methods to equip managers with a more robust understanding of historic and modern fire behaviour. Fire behaviour is assessed using novel methods that can assess soil and rock response to past wildfire heat exposure.

This study examined samples from the 2020 Mangum Fire, in northern Arizona. Sediment and rock were gathered to characterize past fire heating. These samples come from sites with differing soil burn severity (which is a measure of how much the vegetation at the soil surface was destroyed by fire) within the Mangum Fire burn region and sites from outside the fire perimeter.

Luminescence (light) emitted from quartz minerals was analysed following three methods in the lab to detect past heat exposure. Thermally altered rock color (reddening) was also used to assess past heating. This study demonstrates that luminescence signals and rock color measurably alter when heated. These methods may be able to characterize past wildfire heating and provide a more detailed characterization of past fire behaviour. Understanding the difference between past and present fire characteristics can equip land managers to better steward complex ecosystems and the role of fire within these communities.

Alexander Short

Late Pleistocene Piedmont Records in the Grand Staircase Region, Southern Utah

December 2022
Utah State University, Logan, UT
Degree: M.Sc.
Supervisor: Tammy M. Rittenour

Undifferentiated Quaternary alluvial gravel deposits cap sections of the benches of the Grand Staircase in southwestern Utah. Geomorphic position and stratigraphic description suggest these deposits represent the remnants of abandoned piedmont systems and associated terrace sediments deposited during the Pleistocene. Research focuses on the influence of climate and geomorphic processes on late Pleistocene landscape evolution of the Grand Staircase region of southern Utah using piedmont deposits within the five adjoining study catchments as markers of past hillslope sediment supply and river incision. The study catchments are tributaries to the Colorado River and have gradients with base level being controlled by Grand Canyon. The primary hypothesis is that piedmont gravel deposition is driven by climate change and that deposit ages correspond to transitions between glacial and interglacial conditions. Investigation and correlation of piedmont deposits is based on geomorphic analysis, and detailed outcrop and facies descriptions of the sedimentology, stratigraphy, and soil profile development. Age control is provided by optically stimulated luminescence (OSL) dating of representative deposits in each of the study catchments. Deposits of this nature can present a unique set of challenges for OSL dating. Therefore the character of these deposits required the implementation of various sampling techniques.

OSL dating results suggest at minimum three synchronous periods of deposition across the region during the Late Pleistocene (53 ka to > 268 ka) separated by periods of pronounced incision. Accommodating variability between drainage basins, Quaternary alluvial pediments (Qap) can be divided as follows. Qap3 deposits lie 95 to 170 m above the modern channel and were deposited 115 to > 192 ka. Qap2 deposits lie 60 to 75 m above the modern channel and were deposited 69 to 103 ka. Qap1 deposits lie 15 to 25 m above the modern channel and were deposited ~ 53 ka. Secondary, younger and conformable, depositional periods are marked by buried soil horizons identified within Qap3 and Qap2 deposits. A broad comparison of the timing of deposition to regional climate records suggests a response to climate to be the dominant process of Quaternary aggradation and incision of fluvial systems and overall landscape evolution.

A PDF of this thesis can be downloaded from: https://digitalcommons.usu.edu/etd/8651/

Angeli Vasiliki

Dosimetric characterization of new materials with thermally and optically stimulated luminescence for radiation dosimetry

April 2022
Physics Department, Aristotle University of Thessaloniki, Thessaloniki, Greece
Degree: M.Sc.
Supervisors: Professor George Kitis and Dr. George S. Polymeris

This doctoral dissertation is related to a qualitative as well as a quantitative correlation among Thermoluminescence (TL), Blue Optically Stimulated Luminescence (Blue OSL) and Infrared Stimulated Luminescence (IRSL), for different natural dosimetric materials. The geological materials that were used are, a) natural fluorite, CaF_2: N, b) gypsum, c) Durango apatite with two different grain size factions and d) three different K-feldspar samples with code name, ELD1, VRS3 and MRK4; each one belonging to the structural group of microcline, sanidine and orthoclase. The above minerals have been selected due to their specific luminescence characteristics. This work consists of three experimental parts: The first one is attempting the correlation between specific TL glow curves and bleaching components after LM-OSL as well as Blue CW-OSL stimulation, in the case of natural fluorite. The second part includes three materials, Durango apatite, gypsum and one K-feldspar. This part is studying the correlation between the Blue CW-OSL as well as the Residual LM-OSL signal. A two-step stimulation protocol was applied including 10 different IRSL stimulation times, from 0 to 500 s. Finally, the third part is describing the correlation of Blue CW-OSL and IRSL properties of three K-feldspar samples. The stimulation was carried out using Blue CW-OSL and IRSL in two different two-step experimental protocols. The complexity of both recombination pathways as well as the efforts to correlate among the aforementioned luminescence signal was highlighted in the present work.

Bibliography

Compiled by Sebastien Huot

From 1st June 2022 to 30th November 2022

Various geological applications

- aeolian

Bateman, M.D., Bryant, R.G., Luo, W., 2022. Getting the right age? Testing luminescence dating of both quartz and feldspars against independent age controls. Quaternary Geochronology 72, 101366, http://doi.org/10.1016/j.quageo.2022.101366

Chapot, M.S., Duller, G.A.T., Barham, L.S., 2022. Challenges of dating quartz OSL samples with saturated grains: Lessons from single-grain analyses of low dose-rate samples from Victoria Falls, Zambia. Quaternary Geochronology 72, 101344, http://doi.org/10.1016/j.quageo.2022.101344

Li, Z., Wang, F., Luo, C., Liu, C., Wang, X., Yang, S., Ayyamperumal, R., Zhang, J., Li, B., Fan, Y., 2022. Enhanced drying of the Tengger desert, northwest margin of East Asian summer monsoon during warming interglacials after 500 ka. Quaternary Science Reviews 293, 107735, http://doi.org/10.1016/j.quascirev.2022.107735

Moska, P., Sokołowski, R.J., Jary, Z., Zieliński, P., Raczyk, J., Szymak, A., Krawczyk, M., Skurzyński, J., Poręba, G., Łopuch, M., Tudyka, K., 2022. Stratigraphy of the Late Glacial and Holocene aeolian series in different sedimentary zones related to the Last Glacial maximum in Poland. Quaternary International 630, 65-83, http://doi.org/10.1016/j.quaint.2021.04.004

Nottebaum, V., Stauch, G., van der Wal, J.L.N., Zander, A., Schlütz, F., Shumilovskikh, L., Reicherter, K., Batkhishig, O., Lehmkuhl, F., 2022. Late Quaternary landscape evolution and paleoenvironmental implications from multiple geomorphic dryland systems, Orog Nuur Basin, Mongolia. Earth Surface Processes and Landforms 47, 275-297, http://doi.org/10.1002/esp.5247

Peng, J., Wang, X., Yin, G., Adamiec, G., Du, J., Zhao, H., Kang, S., Hu, G., Zheng, Y., 2022. Accumulation of aeolian sediments around the Tengger Desert during the late Quaternary and its implications on interpreting chronostratigraphic records from drylands in north China. Quaternary Science Reviews 275, 107288, http://doi.org/10.1016/j.quascirev.2021.107288

Pflanz, D., Kunz, A., Hornung, J., Hinderer, M., 2022. New insights into the age of aeolian sand deposition in the northern Upper Rhine Graben (Germany). Quaternary International 625, 1-13, http://doi.org/10.1016/j.quaint.2022.03.019

Pincé, P., Vandenberghe, D., Karimi Moayed, N., De Dapper, M., Debeer, A.-E., Van Maldegem, E., Verhegge, J., Piret, L., De Grave, J., Crombé, P., 2022. High-resolution OSL chronology of a well-preserved inland dune in the Lys valley (Sint-Martens-Latem, NW Belgium). Quaternary Geochronology 72, 101322, http://doi.org/10.1016/j.quageo.2022.101322

Robins, L., Roskin, J., Yu, L., Bookman, R., Greenbaum, N., 2022. Aeolian-fluvial processes control landscape evolution along dunefield margins of the northwestern Negev (Israel) since the late Quaternary. Quaternary Science Reviews 285, 107520, http://doi.org/10.1016/j.quascirev.2022.107520

Shandonay, K.L., Bowen, M.W., Larson, P.H., Running, G.L., Rittenour, T., Mataitis, R., 2022. Morphology and stratigraphy of aeolian sand stringers in southeast Minnesota and western Wisconsin, USA. Earth Surface Processes and Landforms 47, 2863-2876, http://doi.org/10.1002/esp.5428

Shen, Q., Ao, S., Xu, Y., Liu, S., Wang, Y., Lai, Y., Miao, X., Lai, Z., 2022. Aeolian landform processes since the last deglaciation revealed by OSL chronology and stratigraphy in the Hulunbuir dune field in NE China. Quaternary Geochronology 72, 101352, http://doi.org/10.1016/j.quageo.2022.101352

Slee, A., McIntosh, P.D., Wang, N., Lounejeva, E., 2022. Aeolian silts indicate the LGM environment in the river Leven valley, Loongana, Tasmania. Quaternary Australasia 39, 22-24, https://search.informit.org/doi/10.3316/informit.529655173421911

Solleiro-Rebolledo, E., Sedov, S., Terhorst, B., López-Martínez, R., Díaz-Ortega, J., Díaz-Hernández, Y., Valera-Fernández, D., Cabadas-Báez, H., Tsukamoto, S., 2022. Late Quaternary paleosols and landscape evolution in dune systems of Veracruz at the Gulf of Mexico coast. Quaternary International 618, 70-86, http://doi.org/10.1016/j.quaint.2021.05.016

Yu, L., Sun, Y., An, P., Greenbaum, N., Roskin, J., 2022. Dunefield expansion and paleoclimate during MIS 3 in the Qaidam Basin, Northeastern Tibetan Plateau: Evidence from Aeolian-Fluvial processes and revised luminescence chronologies. CATENA 215, 106354, http://doi.org/10.1016/j.catena.2022.106354

- alluvial fan

Nir, N., Stahlschmidt, M., Busch, R., Lüthgens, C., Schütt, B., Hardt, J., 2022. Footpaths: Pedogenic and geomorphological long-term effects of human trampling. CATENA 215, 106312, http://doi.org/10.1016/j.catena.2022.106312

- coastal

Andreucci, S., Sechi, D., Buylaert, J.P., Sanna, L., Pascucci, V., 2017. Post-IR IRSL290 dating of K-rich feldspar sand grains in a wind-dominated system on Sardinia. Marine and Petroleum Geology 87, 91-98, http://doi.org/10.1016/j.marpetgeo.2017.03.025

Bateman, M.D., Bryant, R.G., Luo, W., 2022. Getting the right age? Testing luminescence dating of both quartz and feldspars against independent age controls. Quaternary Geochronology 72, 101366, http://doi.org/10.1016/j.quageo.2022.101366

Hu, F., Li, Y., Liang, J., Li, Z., Xie, M., Chen, X., Xiao, Z., 2022. History of coastal dune evolution in the Fujian region of southeastern China over the last millenium. Marine Geology 451, 106878, http://doi.org/10.1016/j.margeo.2022.106878

Köhler, M., Shulmeister, J., Patton, N.R., Rittenour, T.M., McSweeney, S., Ellerton, D.T., Stout, J.C., Hüneke, H., 2021. Holocene evolution of a barrier-spit complex and the interaction of tidal and wave processes, Inskip Peninsula, SE Queensland, Australia. The Holocene 31, 1476-1488, http://doi.org/10.1177/09596836211019092

Kongsen, S., Phantuwongraj, S., Choowong, M., Chawchai, S., Udomsak, S., Chansom, C., Ketthong, C., Surakiatchai, P., Miocic, J.M., Preusser, F., 2022. Multi-proxy approach to identify the origin of high energy coastal deposits from Laem Son National Park, Andaman Sea of Thailand. Quaternary International 625, 82-95, http://doi.org/10.1016/j.quaint.2022.04.017

Liu, P., Zhang, J., Wang, J., Lin, F., Yu, J., Liu, Y., Zhang, D., Sun, Q., Sun, D., Chen, J., Chen, Z., 2022. Tectonic subsidence of the southeast China coast: New evidence from Late Pleistocene transgression in Ningde bay. Palaeogeography, Palaeoclimatology, Palaeoecology 605, 111226, http://doi.org/10.1016/j.palaeo.2022.111226

Nian, X., Zhang, W., Qiu, F., Liu, N., 2022. The complexity of luminescence dating of tidal sand body revealed by the discrepancy of paired quartz OSL ages. Quaternary Geochronology 72, 101347, http://doi.org/10.1016/j.quageo.2022.101347

Okazaki, H., Nara, M., Nakazato, H., Furusawa, A., Ito, K., Tamura, T., 2022. Coastal progradation associated with sea-level oscillations in the later phase of the Last Interglacial period, central Japan. Quaternary Science Reviews 285, 107507, http://doi.org/10.1016/j.quascirev.2022.107507

Park, J., Park, J., Yi, S., Lim, J., Kim, J.C., Jin, Q., Choi, J., 2021. Holocene hydroclimate reconstruction based on pollen, XRF, and grain-size analyses and its implications for past societies of the Korean Peninsula. The Holocene 31, 1489-1500, http://doi.org/10.1177/09596836211019115

Patton, N.R., Shulmeister, J., Rittenour, T.M., Almond, P., Ellerton, D., Santini, T., 2022. Using calibrated surface roughness dating to estimate coastal dune ages at K'gari (Fraser Island) and the Cooloola Sand Mass, Australia. Earth Surface Processes and Landforms 47, 2455-2470, http://doi.org/10.1002/esp.5387

Rodrigues, K., Stapor, F.W., Rink, W.J., Dunbar, J.S., Doran, G., 2022. A 5700-year-old beach-ridge set at Cape Canaveral, Florida, and its implication for Holocene sea-level history in the southeastern USA. The Holocene 32, 40-56, http://doi.org/10.1177/09596836211049975

Seminack, C.T., Thornburg, J.D., Mead, A.J., Mead, H.F., Hadden, C.S., Cherkinsky, A., Nelson, M.S., Patterson, D.B., 2022. Revised temporal and morphostratigraphic context for Clark Quarry: A late-Pleistocene, fluvially-reworked, Atlantic coast backbarrier deposit. Quaternary Science Reviews 284, 107496, http://doi.org/10.1016/j.quascirev.2022.107496

Shtienberg, G., Cantu, K., Mischke, S., Sivan, D., Norris, R.D., Rittenour, T.M., Edelman-Furstenberg, Y., Yasur-Landau, A., Sisma-Ventura, G., Levy, T.E., 2022. Holocene sea-level rise and coastal aquifer interactions: Triggering mechanisms for environmental change and impacts on human settlement patterns at Dor, Israel. Quaternary Science Reviews 294, 107740, http://doi.org/10.1016/j.quascirev.2022.107740

Souza, A.d.O., Lämmle, L., Filho, A.P., Donadio, C., 2022. Recent geomorphological changes in the Paraiba do Sul delta, South America East Coast. Progress in Physical Geography: Earth and Environment 46, 566-588, http://doi.org/10.1177/03091333221077614

Strachan, L.J., Bailleul, J., Bland, K.J., Orpin, A.R., McArthur, A.D., 2022. Pleistocene marine terraces of the Wellington south coast – their distribution across multiple active faults at the southern Hikurangi subduction margin, Aotearoa New Zealand. New Zealand Journal of Geology and Geophysics 65, 1-16, http://doi.org/10.1080/00288306.2021.2011329

Wang, X., Qiu, F., Nian, X., Liu, R., Zhang, W., 2022. Testing the applicability of standardised growth curves (SGCs) for OSL signals of quartz grains from the Yangtze Delta, China. Quaternary Geochronology 72, 101348, http://doi.org/10.1016/j.quageo.2022.101348

Wang, Z., Zheng, H., Meng, X., Zhu, X., Hou, F., Li, J., Mei, X., Wang, Z., Cao, B., Jun, S., 2022. Late Quaternary sedimentation and neotectonics in Liaodong Bay, northern Bohai Sea. Regional Studies in Marine Science 55, 102581, http://doi.org/10.1016/j.rsma.2022.102581

Ward, I.A.K., Bateman, M.D., Larcombe, P., Scott, P.M., Li, T., Murai, K., Khan, N.S., Veth, P., Cullen, P., 2022. A pilot study into the geochronological and geomorphic context for the archaeology of Barrow Island, Western Australia. Quaternary International 638-639, 5-22, http://doi.org/10.1016/j.quaint.2022.02.002

Waselkov, G.A., Beebe, D.A., Cyr, H., Chamberlain, E.L., Mehta, J.M., Nelson, E.S., 2022. History and Hydrology: Engineering Canoe Canals in the Estuaries of the Gulf of Mexico. Journal of Field Archaeology 47, 486-500, http://doi.org/10.1080/00934690.2022.2090747

Wu, Y., Huang, X., Zheng, X., Meadows, M.E., Wang, Z., 2022. Sedimentary records of mid-Holocene extreme storm events on the north bank of Hangzhou Bay, East China. Marine Geology 451, 106891, http://doi.org/10.1016/j.margeo.2022.106891

Yang, D.-Y., Han, M., Yoon, H.H., Cho, A., Kim, J.C., Choi, E., Kashima, K., 2022. Early Holocene relative sea-level changes on the central east coast of the Yellow Sea. Palaeogeography, Palaeoclimatology, Palaeoecology 603, 111185, http://doi.org/10.1016/j.palaeo.2022.111185

Yongqing, R., Jianhui, J., Yunming, H., Xinxin, Z., 2022. Chronology of Last Glacial Maximum sediments in the coast of Fujian, South China. Marine Geology 451, 106884, http://doi.org/10.1016/j.margeo.2022.106884

Zaretskaya, N., Korsakova, O., Molodkov, A., Ruchkin, M., Baranov, D., Rybalko, A., Lugovoy, N., Merkuliev, A., 2022. Early Middle Weichselian in the White Sea and adjacent areas: Chronology, stratigraphy and palaeoenvironments. Quaternary International 632, 65-78, http://doi.org/10.1016/j.quaint.2022.05.007

- colluvial

McCarroll, N.R., Pederson, J.L., Hidy, A.J., Rittenour, T.M., 2021. Chronostratigraphy of talus flatirons and piedmont alluvium along the Book Cliffs, Utah – Testing models of dryland escarpment evolution. Quaternary Science Reviews 274, 107286, http://doi.org/10.1016/j.quascirev.2021.107286

Peñuela, A., Hayas, A., Infante-Amate, J., Ruiz-Montes, P., Temme, A., Reimann, T., Peña-Acevedo, A., Vanwalleghem, T., 2023. A multi-millennial reconstruction of gully erosion in two contrasting Mediterranean catchments. CATENA 220, 106709, http://doi.org/10.1016/j.catena.2022.106709

- earthquake (and fault related)

Chupik, C., Koehler, R., Keen-Zebert, A., 2022. Complex Holocene Fault Ruptures on the Warm Springs Valley Fault in the Northern Walker Lane, Nevada–Northern California. Bulletin of the Seismological Society of America 112, 575-596, http://doi.org/10.1785/0120200271

Huang, X., Lai, Z., Xu, L., Luo, L., Zhong, J., Xie, J., Zhou, Y., Granger, D.E., 2022. Late Pleistocene lake overspill and drainage reversal in the source area of the Yellow River in the Tibetan Plateau. Earth and Planetary Science Letters 589, 117554, http://doi.org/10.1016/j.epsl.2022.117554

Liang, L., Zhang, Z., Dai, F., 2022. A Late Pleistocene landslide damming event and its implications for the evolution of river valley landforms in the upper Jinsha River, southeastern Tibetan Plateau. Quaternary International 622, 97-109, http://doi.org/10.1016/j.quaint.2022.01.006

Mokatse, T., Vainer, S., Irving, J., Schmidt, C., Kgosidintsi, B., Shemang, E., Verrecchia, E.P., 2022. Geometry of sedimentary deposits and evolution of the landforms in the Chobe Enclave, Northern Botswana. Geomorphology 415, 108406, http://doi.org/10.1016/j.geomorph.2022.108406

Pisarska-Jamroży, M., Belzyt, S., Börner, A., Hoffmann, G., Kenzler, M., Rother, H., Steffen, R., Steffen, H., 2022. Late Pleistocene earthquakes imprinted on glaciolacustrine sediments on Gnitz Peninsula (Usedom Island, NE Germany). Quaternary Science Reviews 296, 107807, http://doi.org/10.1016/j.quascirev.2022.107807

Puliti, I., Pucci, S., Villani, F., Porreca, M., Benedetti, L., Robustelli, G., Gueli, A., Stella, G., 2022. Estimating the long-term slip rate of active normal faults: The case of the Paganica Fault (Central Apennines, Italy). Geomorphology 415, 108411, http://doi.org/10.1016/j.geomorph.2022.108411

Regalla, C., Kirby, E., Mahan, S., McDonald, E., Pangrcic, H., Binkley, A., Schottenfels, E., LaPlante, A., Sethanant, I., Lynch, E.M., 2022. Late Holocene rupture history of the Ash Hill fault, Eastern California Shear Zone, and the potential for seismogenic strain transfer between nearby faults. Earth Surface Processes and Landforms 47, 2897-2925, http://doi.org/10.1002/esp.5432

Štěpančíková, P., Rockwell, T.K., Stemberk, J., Rhodes, E.J., Hartvich, F., Luttrell, K., Myers, M., Táborík, P., Rood, D.H., Wechsler, N., Nývlt, D., Ortuño, M., Hók, J., 2022. Acceleration of Late Pleistocene activity of a Central European fault driven by ice loading. Earth and Planetary Science Letters 591, 117596, http://doi.org/10.1016/j.epsl.2022.117596

Zhang, H., Zhang, X., Liu, W., Yeh, P.J.F., Ye, P., He, X., 2022. Impacts of active tectonics on geogenic arsenic enrichment in groundwater in the Hetao Plain, Inner Mongolia. Quaternary Science Reviews 278, 107343, http://doi.org/10.1016/j.quascirev.2021.107343

- fluvial

Gao, L., Long, H., Hou, Y., Feng, Y., 2022. Chronology constraints on the complex sedimentary stratigraphy of the paleo-Yangtze incised valley in China. Quaternary Science Reviews 287, 107573, http://doi.org/10.1016/j.quascirev.2022.107573

Guyez, A., Bonnet, S., Reimann, T., Carretier, S., Wallinga, J., 2022. Illuminating past river incision, sediment source and pathways using luminescence signals of individual feldspar grains (Rangitikei River, New Zealand). Earth Surface Processes and Landforms 47, 1952-1971, http://doi.org/10.1002/esp.5357

Jones, M.D., Richter, T., Rollefson, G., Rowan, Y., Roe, J., Toms, P., Wood, J., Wasse, A., Ikram, H., Williams, M., AlShdaifat, A., Pedersen, P.N., Esaid, W., 2022. The palaeoenvironmental potential of the eastern Jordanian desert basins (Qe'an). Quaternary International 635, 73-82, http://doi.org/10.1016/j.quaint.2021.06.023

Liu, Q., Chen, J., Qin, J., Yang, H., Di, N., Liu, J., Zhang, W., 2022. MET-post-IR IRSL luminescence dating of cobbles buried in fluvial terraces in the Northern Chinese Tian Shan. Quaternary Geochronology 72, 101351, http://doi.org/10.1016/j.quageo.2022.101351

Lu, P., Xu, J., Zhuang, Y., Chen, P., Wang, H., Tian, Y., Mo, D., Gu, W., Yang, R., Wang, X., Zhou, L., Li, Y., Zhang, X., Li, Y., 2022. Prolonged landscape stability sustained the continuous development of ancient civilizations in the Shuangji River valley of China's Central Plains. Geomorphology 413, 108359, http://doi.org/10.1016/j.geomorph.2022.108359

Macklin, M.G., Booth, J., Brewer, P.A., Tooth, S., Duller, G.A.T., 2022. How have Cretan rivers responded to late Holocene uplift? A multi-millennial, multi-catchment field experiment to evaluate the applicability of Schumm and Parker's (1973) complex response model. Earth Surface Processes and Landforms 47, 2178-2197, http://doi.org/10.1002/esp.5370

Mokatse, T., Vainer, S., Irving, J., Schmidt, C., Kgosidintsi, B., Shemang, E., Verrecchia, E.P., 2022. Geometry of sedimentary deposits and evolution of the landforms in the Chobe Enclave, Northern Botswana. Geomorphology 415, 108406, http://doi.org/10.1016/j.geomorph.2022.108406

Narzary, B., Singh, A.K., Malik, S., Mahadev, Jaiswal, M.K., 2022. Luminescence chronology of the Sankosh river terraces in the Assam- Bhutan foothills of the Himalayas: Implications to climate and tectonics. Quaternary Geochronology 72, 101364, http://doi.org/10.1016/j.quageo.2022.101364

Robins, L., Roskin, J., Yu, L., Bookman, R., Greenbaum, N., 2022. Aeolian-fluvial processes control landscape evolution along dunefield margins of the northwestern Negev (Israel) since the late Quaternary. Quaternary Science Reviews 285, 107520, http://doi.org/10.1016/j.quascirev.2022.107520

Seminack, C.T., Thornburg, J.D., Mead, A.J., Mead, H.F., Hadden, C.S., Cherkinsky, A., Nelson, M.S., Patterson, D.B., 2022. Revised temporal and morphostratigraphic context for Clark Quarry: A late-Pleistocene, fluvially-reworked, Atlantic coast backbarrier deposit. Quaternary Science Reviews 284, 107496, http://doi.org/10.1016/j.quascirev.2022.107496

Sodhi, A., Das, A., Prizomwala, S.P., Vedpathak, C., Makwana, N., 2022. Centennial-scale linkages between the Indian Summer Monsoon and the solar irradiation from the Gulf of Khambhat (Western India). Quaternary International 631, 82-92, http://doi.org/10.1016/j.quaint.2022.05.011

Taormina, R., Nordt, L., Bateman, M., 2022. Late quaternary alluvial history of the Brazos River in central Texas. Quaternary International 631, 34-46, http://doi.org/10.1016/j.quaint.2022.05.008

Taratunina, N.A., Buylaert, J.P., Kurbanov, R.N., Yanina, T.A., Makeev, A.O., Lebedeva, M.P., Utkina, A.O., Murray, A.S., 2022. Late Quaternary evolution of lower reaches of the Volga River (Raygorod section) based on luminescence dating. Quaternary Geochronology 72, 101369, http://doi.org/10.1016/j.quageo.2022.101369

Tooth, S., McCarthy, T.S., Duller, G.A.T., Assine, M.L., Wolski, P., Coetzee, G., 2022. Significantly enhanced mid Holocene fluvial activity in a globally important, arid-zone wetland: The Okavango Delta, Botswana. Earth Surface Processes and Landforms 47, 854-871, http://doi.org/10.1002/esp.5289

Walsh, E., Caracciolo, L., Ravidà, D., Burrough, S., Thomas, D., 2022. Holocene fluvial depositional regimes of the Huab River, Skeleton Coast, Namibia. Earth Surface Processes and Landforms 47, 1820-1844, http://doi.org/10.1002/esp.5349

Yang, J., Xia, D., Chen, Z., Wang, S., Gao, F., Liu, X., Zhao, S., Zhao, L., Liu, Y., 2023. Differentiating detrital and pedogenic contributions to the magnetic properties of aeolian deposits in the southern Tibetan Plateau: Implications for paleoclimatic reconstruction. CATENA 220, 106736, http://doi.org/10.1016/j.catena.2022.106736

Yang, X., Yu, L., Chang, Q., Lai, Z., 2022. Flood activity revealed millennial-scale climatic changes during the late Holocene in the Qaidam Basin, northeastern Tibetan Plateau. Quaternary International 637, 32-43, http://doi.org/10.1016/j.quaint.2022.06.011

Zaki, A.S., King, G.E., Haghipour, N., Giegengack, R., Watkins, S.E., Gupta, S., Schuster, M., Khairy, H., Ahmed, S., El-Wakil, M., Eltayeb, S.A., Herman, F., Castelltort, S., 2021. Did increased flooding during the African Humid Period force migration of modern humans from the Nile Valley? Quaternary Science Reviews 272, 107200, http://doi.org/10.1016/j.quascirev.2021.107200

Zondervan, J.R., Stokes, M., Telfer, M.W., Boulton, S.J., Mather, A.E., Buylaert, J.-P., Jain, M., Murray, A.S., Belfoul, M.A., 2022. Constraining a model of punctuated river incision for Quaternary strath terrace formation. Geomorphology 414, 108396, http://doi.org/10.1016/j.geomorph.2022.108396

- glacial and periglacial

Ali, S.N., Singh, P., Arora, P., Bisht, P., Morthekai, P., 2022. Luminescence dating of late pleistocene glacial and glacio-fluvial sediments in the Central Himalaya, India. Quaternary Science Reviews 284, 107464, http://doi.org/10.1016/j.quascirev.2022.107464

Clark, C.D., Ely, J.C., Hindmarsh, R.C.A., Bradley, S., Ignéczi, A., Fabel, D., Ó Cofaigh, C., Chiverrell, R.C., Scourse, J., Benetti, S., Bradwell, T., Evans, D.J.A., Roberts, D.H., Burke, M., Callard, S.L., Medialdea, A., Saher, M., Small, D., Smedley, R.K., Gasson, E., Gregoire, L., Gandy, N., Hughes, A.L.C., Ballantyne, C., Bateman, M.D., Bigg, G.R., Doole, J., Dove, D., Duller, G.A.T., Jenkins, G.T.H., Livingstone, S.L., McCarron, S., Moreton, S., Pollard, D., Praeg, D., Sejrup, H.P., Van Landeghem, K.J.J., Wilson, P., 2022. Growth and retreat of the last British–Irish Ice Sheet, 31 000 to 15 000 years ago: the BRITICE-CHRONO reconstruction. Boreas 51, 699-758, http://doi.org/10.1111/bor.12594

Gibson, S.M., Bateman, M.D., Murton, J.B., Barrows, T.T., Fifield, L.K., Gibbard, P.L., 2022. Timing and dynamics of Late Wolstonian Substage 'Moreton Stadial' (MIS 6) glaciation in the English West Midlands, UK. Royal Society Open Science 9, 220312, http://doi.org/10.1098/rsos.220312

Gómez, G.A., García, J.-L., Villagrán, C., Lüthgens, C., Abarzúa, A.M., 2022. Vegetation, glacier, and climate changes before the global last glacial maximum in the Isla Grande de Chiloé, southern Chile (42° S). Quaternary Science Reviews 276, 107301, http://doi.org/10.1016/j.quascirev.2021.107301

Gromig, R., Lebas, E., Savelieva, L., Pushina, Z., Fedorov, G., Brill, D., Lenz, M.M., Krastel, S., Wagner, B., Kostromina, N., Mustafin, M., Melles, M., 2022. Sedimentation history of Lake Taymyr, Central Russian Arctic, since the Last Glacial Maximum. Journal of Quaternary Science 37, 851-867, http://doi.org/10.1002/jqs.3342

Hu, K., Wei, L., Yang, A., Wu, C., Zhang, Q., Liu, S., Wang, Z., 2022. Broad valleys and barrier dams in upstream Brahmaputra efficiently retain Tibetan-sourced sediments: Evidence from palaeoflood records. Quaternary Science Reviews 285, 107538, http://doi.org/10.1016/j.quascirev.2022.107538

Leger, T.P.M., Hein, A.S., Bingham, R.G., Rodés, Á., Fabel, D., Smedley, R.K., 2021. Geomorphology and 10Be chronology of the Last Glacial Maximum and deglaciation in northeastern Patagonia, 43°S-71°W. Quaternary Science Reviews 272, 107194, http://doi.org/10.1016/j.quascirev.2021.107194

Lenz, M., Lenz, M.M., Andreev, A., Scheidt, S., Gromig, R., Lebas, E., Fedorov, G., Krastel, S., Melles, M., Wagner, B., 2022. Climate and environmental history at Lake Levinson-Lessing, Taymyr Peninsula, during the last 62 kyr. Journal of Quaternary Science 37, 836-850, http://doi.org/10.1002/jqs.3384

Lenz, M.M., Andreev, A., Nazarova, L., Syrykh, L.S., Scheidt, S., Haflidason, H., Meyer, H., Brill, D., Wagner, B., Gromig, R., Lenz, M., Rolf, C., Kuhn, G., Fedorov, G., Svendsen, J.I., Melles, M., 2022. Climate, glacial and vegetation history of the polar Ural Mountains since c. 27 cal ka bp, inferred from a 54 m long sediment core from Lake Bolshoye Shchuchye. Journal of Quaternary Science 37, 818-835, http://doi.org/10.1002/jqs.3400

Luczak, J.N., Fisher, T.G., Lepper, K., 2022. Chronology and stratigraphy of the Imlay Channel in Lapeer County, Michigan, USA. Canadian Journal of Earth Sciences 59, 59-70, http://doi.org/10.1139/cjes-2021-0039

Nazarov, D.V., Nikolskaia, O.A., Zhigmanovskiy, I.V., Ruchkin, M.V., Cherezova, A.A., 2022. Lake Yamal, an ice-dammed megalake in the West Siberian Arctic during the Late Pleistocene, ~60–35 ka. Quaternary Science Reviews 289, 107614, http://doi.org/10.1016/j.quascirev.2022.107614

Pisarska-Jamroży, M., Belzyt, S., Börner, A., Hoffmann, G., Kenzler, M., Rother, H., Steffen, R., Steffen, H., 2022. Late Pleistocene earthquakes imprinted on glaciolacustrine sediments on Gnitz Peninsula (Usedom Island, NE Germany). Quaternary Science Reviews 296, 107807, http://doi.org/10.1016/j.quascirev.2022.107807

Serra, E., Valla, P.G., Gribenski, N., Carcaillet, J., Deline, P., 2022. Post-LGM glacial and geomorphic evolution of the Dora Baltea valley (western Italian Alps). Quaternary Science Reviews 282, 107446, http://doi.org/10.1016/j.quascirev.2022.107446

Shrivastava, P.K., Singh, G., Thapa, S.J., Chunchekar, R., Srivastava, H.B., Mugal, V.V., 2022. Late Quaternary geomorphic evolution of Teesta-Khangtse basin, north Sikkim. Polar Science 34, 100868, http://doi.org/10.1016/j.polar.2022.100868

Štěpančíková, P., Rockwell, T.K., Stemberk, J., Rhodes, E.J., Hartvich, F., Luttrell, K., Myers, M., Tábořík, P., Rood, D.H., Wechsler, N., Nývlt, D., Ortuño, M., Hók, J., 2022. Acceleration of Late Pleistocene activity of a Central European fault driven by ice loading. Earth and Planetary Science Letters 591, 117596, http://doi.org/10.1016/j.epsl.2022.117596

Uścinowicz, S., Adamiec, G., Bluszcz, A., Jegliñski, W., Jurys, L., Miotk-Szpiganowicz, G., Moska, P., Paczek, U., Piotrowska, N., Porêba, G., Przezdziecki, P., Uoecinowicz, G., 2019. Chronology of the last ice sheet decay on the southern Baltic area based on dating of glaciofluvial and ice-dammed lake deposits. Geological Quarterly 63, 193-208, http://doi.org/10.7306/gq.1453

Włodarski, W., Szuman, I., Kalita, J.Z., Ewertowski, M.W., Alexanderson, H., 2022. The interplay between deformation and deposition in a Pleistocene push moraine: New insight from structural interpretation and area-depth-strain analysis of the growth strata. Sedimentary Geology 437, 106192, http://doi.org/10.1016/j.sedgeo.2022.106192

Zhang, S., Zhao, H., Sheng, Y., Zhang, J., Zhang, J., Sun, A., Wang, L., Huang, L., Hou, J., Chen, F., 2022. Mega-lakes in the northwestern Tibetan Plateau formed by melting glaciers during the last deglacial. Quaternary Science Reviews 285, 107528, http://doi.org/10.1016/j.quascirev.2022.107528

- lacustrine

Adolph, M.-L., Lampe, R., Lorenz, S., Haberzettl, T., 2022. Characterization of (paleo)lacustrine landforms using sedimentological and portable OSL investigations at Schweriner See, north-eastern Germany. Earth Surface Processes and Landforms 47, 422-435, http://doi.org/10.1002/esp.5258

Burrough, S.L., Thomas, D.S.G., Allin, J.R., Coulson, S.D., Mothulatshipi, S.M., Nash, D.J., Staurset, S., 2022. Lessons from a lakebed: unpicking hydrological change and early human landscape use in the Makgadikgadi basin, Botswana. Quaternary Science Reviews 291, 107662, http://doi.org/10.1016/j.quascirev.2022.107662

Cohen, T.J., Arnold, L.J., Gázquez, F., May, J.-H., Marx, S.K., Jankowski, N.R., Chivas, A.R., Garćia, A., Cadd, H., Parker, A.G., Jansen, J.D., Fu, X., Waldmann, N., Nanson, G.C., Jones, B.G., Gadd, P., 2022. Late Quaternary climate change in Australia's arid interior: Evidence from Kati Thanda – Lake Eyre. Quaternary Science Reviews 292, 107635, http://doi.org/10.1016/j.quascirev.2022.107635

Gao, L., Xiao, X., Li, Y., Jiang, Q., Long, H., 2022. Chronological constraints on the late Quaternary Beihai wetland deposits in southwestern China and its depositional history linked to hydroclimate change. Palaeogeography, Palaeoclimatology, Palaeoecology 599, 111047, http://doi.org/10.1016/j.palaeo.2022.111047

Guo, X., Wei, J., Song, Z., 2022. Luminescence dating of a dammed lake formed by Ashegong landslide on the northeastern Tibetan Plateau. Quaternary International 629, 74-80, http://doi.org/10.1016/j.quaint.2020.11.050

Heyer, J., Brewer, S., Brunelle, A., Leys, B., Lundeen, Z., Rittenour, T., Power, M., 2022. Age control for the Lake Bottom oxbow in the Dolores River watershed of eastern Utah, USA. Quaternary International 621, 62-73, http://doi.org/10.1016/j.quaint.2020.09.013

Huang, C., Guo, Y., Yu, L., Cao, M., Tu, H., Lai, Z., 2023. Holocene hydrological history of a Tibetan glacier-fed lake Taro Co in response to climate change. CATENA 220, 106686, http://doi.org/10.1016/j.catena.2022.106686

Huang, X., Lai, Z., Xu, L., Luo, L., Zhong, J., Xie, J., Zhou, Y., Granger, D.E., 2022. Late Pleistocene lake overspill and drainage reversal in the source area of the Yellow River in the Tibetan Plateau. Earth and Planetary Science Letters 589, 117554, http://doi.org/10.1016/j.epsl.2022.117554

Jena, P.S., Bhushan, R., Raj, H., Dabhi, A.J., Sharma, S., Shukla, A.D., Juyal, N., 2022. Relict proglacial lake of Spituk (Leh), northwest (NW) Himalaya: A repository of hydrological changes during Marine Isotopic Stage (MIS)-2. Palaeogeography, Palaeoclimatology, Palaeoecology 602, 111164, http://doi.org/10.1016/j.palaeo.2022.111164

Li, G., Wang, X., Zhang, X., Yan, Z., Liu, Y., Yang, H., Wang, Y., Jonell, T.N., Qian, J., Gou, S., Yu, L., Wang, Z., Chen, J., 2022. Westerlies-Monsoon interaction drives out-of-phase precipitation and asynchronous lake level changes between Central and East Asia over the last millennium. CATENA 218, 106568, http://doi.org/10.1016/j.catena.2022.106568

Liu, X., Wang, Y., Miao, X., Ou, X., Zheng, C., Xu, Y., Lai, Z., 2022. Holocene lake level variations of Dagze Co in central Tibetan Plateau revealed by OSL dates on palaeoshorelines. CATENA 219, 106645, http://doi.org/10.1016/j.catena.2022.106645

Nottebaum, V., Stauch, G., van der Wal, J.L.N., Zander, A., Schlütz, F., Shumilovskikh, L., Reicherter, K., Batkhishig, O., Lehmkuhl, F., 2022. Late Quaternary landscape evolution and paleoenvironmental implications from multiple geomorphic dryland systems, Orog Nuur Basin, Mongolia. Earth Surface Processes and Landforms 47, 275-297, http://doi.org/10.1002/esp.5247

Roberts, H.M., Ramsey, C.B., Chapot, M.S., Deino, A.L., Lane, C.S., Vidal, C., Asrat, A., Cohen, A., Foerster, V., Lamb, H.F., Schäbitz, F., Trauth, M.H., Viehberg, F.A., 2021. Using multiple chronometers to establish a long, directly-dated lacustrine record: Constraining >600,000 years of environmental change at Chew Bahir, Ethiopia. Quaternary Science Reviews 266, 107025, http://doi.org/10.1016/j.quascirev.2021.107025

Zhang, S., Zhao, H., Sheng, Y., Chen, S., Li, G., Chen, F., 2022. Late Quaternary lake level record of Orog Nuur, southern Mongolia, revealed by optical dating of paleo-shorelines. Quaternary Geochronology 72, 101370, http://doi.org/10.1016/j.quageo.2022.101370

- loess

Coppo, R., Cosentino, N.J., Torre, G., del Rio, I., Sawakuchi, A.O., Berman, A.L., Koester, E., Delmonte, B., Gaiero, D.M., 2022. Coeval minimum south American and maximum Antarctic last glacial maximum dust deposition: A causal link? Quaternary Science Reviews 295, 107768, http://doi.org/10.1016/j.quascirev.2022.107768

Fenn, K., Thomas, D.S.G., Durcan, J.A., Millar, I.L., Veres, D., Piermattei, A., Lane, C.S., 2021. A tale of two signals: Global and local influences on the Late Pleistocene loess sequences in Bulgarian Lower Danube. Quaternary Science Reviews 274, 107264, http://doi.org/10.1016/j.quascirev.2021.107264

Łanczont, M., Madeyska, T., Mroczek, P., Komar, M., Hołub, B., Standzikowski, K., Fedorowicz, S., 2023. Reconstruction of the environmental conditions during the earliest Palaeolithic occupations in the Podillia Upland (W Ukraine) and the formation of archaeological layers. CATENA 221, 106753, http://doi.org/10.1016/j.catena.2022.106753

Łanczont, M., Mroczek, P., Komar, M., Fedorowicz, S., Woronko, B., Nawrocki, J., Frankowski, Z., Standzikowski, K., 2022. A remarkable last glacial loess sedimentation at Roxolany in the Dniester Liman (Southern Ukraine). Quaternary Science Reviews 285, 107521, http://doi.org/10.1016/j.quascirev.2022.107521

Li, J., Yang, L.-R., 2022. Variations in the sensitivity of the optically stimulated luminescence from quartz in the Xifeng section: A spatiotemporal comparison across the Chinese Loess Plateau since the last interglaciation. Quaternary Geochronology 72, 101353, http://doi.org/10.1016/j.quageo.2022.101353

Liu, L., Yang, S., Liu, X., Cheng, T., Li, P., Zhou, J., Chen, Z., Luo, Y., 2022. Effects of the size of the test dose on the SAR protocol for quartz optically stimulated luminescence dating of loess in the eastern Tibetan Plateau. Quaternary Geochronology 72, 101365, http://doi.org/10.1016/j.quageo.2022.101365

Loba, A., Zhang, J., Tsukamoto, S., Kasprzak, M., Beata Kowalska, J., Frechen, M., Waroszewski, J., 2023. Multiproxy approach to the reconstruction of soil denudation events and the disappearance of Luvisols in the loess landscape of south-western Poland. CATENA 220, 106724, http://doi.org/10.1016/j.catena.2022.106724

Niu, Y., Fan, Y., Qiao, Y., Lü, T., Li, C., Qi, L., Wang, S., Peng, S., Tan, Y., 2022. Chronostratigraphy of a loess-paleosol sequence in the western Chinese Loess Plateau based on ESR dating and magnetostratigraphy. Quaternary International 637, 1-11, http://doi.org/10.1016/j.quaint.2022.08.005

Stevens, T., Sechi, D., Tziavaras, C., Schneider, R., Banak, A., Andreucci, S., Hättestrand, M., Pascucci, V., 2022. Age, formation and significance of loess deposits in central Sweden. Earth Surface Processes and Landforms 47, 3276-3301, http://doi.org/10.1002/esp.5456

Sümegi, P., Molnár, D., Gulyás, S., Stevens, T., Makó, L., Cseh, P., Molnár, M., Fitzsimmons, K., Nett, J.J., Hlavatskyi, D., Lehmkuhl, F., 2022. Comparison of High-Resolution 14C and Luminescence-Based Chronologies of the MIS 2 Madaras Loess/Paleosol Sequence, Hungary: Implications for Chronological Studies. Quaternary 5, 47, http://doi.org/10.3390/quat5040047

Sychev, N.V., Konstantinov, E.A., Zakharov, A.L., Frechen, M., Tsukamoto, S., 2022. New data on geochronology of the upper Quaternary loess–soil series in the Terek–Kuma lowland. Lithology and Mineral Resources 57, 336-347, http://doi.org/10.1134/S0024490222040071

Timireva, S.N., Kononov, Y.M., Sycheva, S.A., Taratunina, N.A., Kalinin, P.I., Filippova, K.G., Zakharov, A.L., Konstantinov, E.A., Murray, A.S., Kurbanov, R.N., 2022. Revisiting the Taman peninsula loess-paleosol sequence: Middle and Late Pleistocene record of Cape Pekla. Quaternary International 620, 36-45, http://doi.org/10.1016/j.quaint.2021.06.010

Volvakh, A.O., Volvakh, N.E., Ovchinnikov, I.Y., Smolyaninova, L.G., Kurbanov, R.N., 2022. Loess-paleosol record of MIS 3 - MIS 2 of north-east Cis-Salair plain, south of West Siberia. Quaternary International 620, 58-74, http://doi.org/10.1016/j.quaint.2021.06.026

Yi, S., Zeng, L., Xu, Z., Wang, Y., Wang, X., Wu, J., Lu, H., 2022. Sea-level changes in the Bohai Sea, northern China, constrained by coastal loess accumulation over the past 200 ka. Quaternary Science Reviews 277, 107368, http://doi.org/10.1016/j.quascirev.2021.107368

- soil

Cao, Z., Ke, Q., Zhang, K., Zhang, Z., Liu, Y., Xiao, S., Wei, M., 2022. Millennial scale erosion and sedimentation investigation in karst watersheds using dating and palynology. CATENA 217, 106526, http://doi.org/10.1016/j.catena.2022.106526

Nelson, M.S., Eppes, M.C., Rittenour, T.M., 2022. Quartz luminescence sensitivity from sediment versus bedrock in highly weathered soils of the Piedmont of North Carolina, south-eastern USA. Quaternary Geochronology 72, 101343, http://doi.org/10.1016/j.quageo.2022.101343

- surface exposure dating

Ageby, L., Angelucci, D.E., Brill, D., Carrer, F., Brückner, H., Klasen, N., 2022. Dating dry-stone walls with rock surface luminescence: A case study from the Italian Alps. Journal of Archaeological Science 144, 105625, http://doi.org/10.1016/j.jas.2022.105625

Bench, T., Feathers, J., 2022. Trialing the application of controlled exposure experiments for optical exposure dating on quartzite quarry surfaces in Washington State. Radiation Measurements 156, 106805, http://doi.org/10.1016/j.radmeas.2022.106805

Cui, F., Qin, J., Liu, J., Fan, P., Li, Z., Li, K., Chen, J., 2022. Isolating quartz-dominated OSL signal of rock slice by using pulsed stimulation: Implications for dating burial age of cobbles. Quaternary Geochronology 72, 101367, http://doi.org/10.1016/j.quageo.2022.101367

Feathers, J.K., Aaberg, S., Chase, J., Kennedy, M., Peterson, L., Reeves, B., Wagers, S., 2022. Dating stone arrangements using luminescence: More data from the northern Great Plains. Plains Anthropologist 67, 297-322, http://doi.org/10.1080/00320447.2022.2100618

Liu, Q., Chen, J., Qin, J., Yang, H., Di, N., Liu, J., Zhang, W., 2022. MET-post-IR IRSL luminescence dating of cobbles buried in fluvial terraces in the Northern Chinese Tian Shan. Quaternary Geochronology 72, 101351, http://doi.org/10.1016/j.quageo.2022.101351

Ou, X.J., Roberts, H.M., Duller, G.A.T., 2022. Rapid assessment of beta dose variation inside cobbles, and implications for rock luminescence dating. Quaternary Geochronology 72, 101349, http://doi.org/10.1016/j.quageo.2022.101349

Thompson, W.K., Arvidsson, D., Murray, A.S., Blidberg, A., Hansen, V., 2022. Rock and sediment luminescence dating of an ancient circular stone-walled enclosure at Sønnebøe, northern Scania, Sweden. Quaternary Geochronology 72, 101340, http://doi.org/10.1016/j.quageo.2022.101340

- unclassified environment

Strobel, P., Bliedtner, M., Carr, A.S., Struck, J., du Plessis, N., Glaser, B., Meadows, M.E., Quick, L.J., Zech, M., Zech, R., Haberzettl, T., 2022. Reconstructing Late Quaternary precipitation and its source on the southern Cape coast of South Africa: A multi-proxy paleoenvironmental record from Vankervelsvlei. Quaternary Science Reviews 284, 107467, http://doi.org/10.1016/j.quascirev.2022.107467

Archaeology applications

Allen, P., Bain, D.R., Bridgland, D.R., Buisson, P., Buylaert, J.-P., Bynoe, R., George, W.H., Haggart, B.A., Horne, D.J., Littlewood, E.-M., Lord, A.R., March, A.C., Mercer, I., Mercer, R., Murray, A.S., Penkman, K.E.H., Preece, R.C., Ratford, J., Schreve, D.C., Snelling, A.J.R., Sohar, K., Whittaker, J., White, M.J., White, T.S., 2022. Mid-Late Quaternary Fluvial Archives near the Margin of the MIS 12 Glaciation in Southern East Anglia, UK: Amalgamation of Multi-Disciplinary and Citizen-Science Data Sources. Quaternary 5, http://doi.org/10.3390/quat5030037

Ames, C.J.H., Cordova, C.E., Boyd, K., Schmidt, C., Degering, D., Kalbe, J., Jones, B.G., Dosseto, A., Pokines, J.T., Alsouliman, A.S., Beller, J.A., Nowell, A., 2022. Middle to Late Quaternary palaeolandscapes of the central Azraq Basin, Jordan: Deciphering discontinuous records of human-environment dynamics at the arid margin of the Levant. Quaternary International 635, 31-52, http://doi.org/10.1016/j.quaint.2021.10.007

Barzilai, O., Abulafia, T., Shemer, M., May, H., Orbach, M., Frumkin, A., Yeshurun, R., Sarig, R., Porat, N., Hershkovitz, I., 2022. Rediscovering Geula Cave: A Middle Paleolithic cave site in northern Mt. Carmel, Israel. Quaternary International 624, 181-197, http://doi.org/10.1016/j.quaint.2021.03.007

Burrough, S.L., Thomas, D.S.G., Allin, J.R., Coulson, S.D., Mothulatshipi, S.M., Nash, D.J., Staurset, S., 2022. Lessons from a lakebed: unpicking hydrological change and early human landscape use in the Makgadikgadi basin, Botswana. Quaternary Science Reviews 291, 107662, http://doi.org/10.1016/j.quascirev.2022.107662

Feathers, J.K., Aaberg, S., Chase, J., Kennedy, M., Peterson, L., Reeves, B., Wagers, S., 2022. Dating stone arrangements using luminescence: More data from the northern Great Plains. Plains Anthropologist 67, 297-322, http://doi.org/10.1080/00320447.2022.2100618

Frouin, M., Douka, K., Dave, A.K., Schwenninger, J.-L., Mercier, N., Murray, A.S., Santaniello, F., Boschian, G., Grimaldi, S., Higham, T., 2022. A refined chronology for the Middle and early Upper Paleolithic sequence of Riparo Mochi (Liguria, Italy). Journal of Human Evolution 169, 103211, http://doi.org/10.1016/j.jhevol.2022.103211

Guagnin, M., Charloux, G., AlSharekh, A.M., Crassard, R., Hilbert, Y.H., Andreae, M.O., AlAmri, A., Preusser, F., Dubois, F., Burgos, F., Flohr, P., Mora, P., AlQaeed, A., AlAli, Y., 2022. Life-sized Neolithic camel sculptures in Arabia: A scientific assessment of the craftsmanship and age of the Camel Site reliefs. Journal of Archaeological Science: Reports 42, 103165, http://doi.org/10.1016/j.jasrep.2021.103165

Heydari, M., Guérin, G., Sirakov, N., Fernandez, P., Ferrier, C., Guadelli, A., Leblanc, J.-C., Taneva, S., Sirakova, S., Guadelli, J.-L., 2022. The last 30,000 to 700,000 years ago: Unravelling the timing of human settlement for the Palaeolithic site of Kozarnika. Quaternary Science Reviews 291, 107645, http://doi.org/10.1016/j.quascirev.2022.107645

Khamsiri, S., Venunan, P., Khaokheiw, C., Silapanth, P., Banron, S., Pailoplee, S., 2022. Late iron-smelting production of Angkor Highland, metallurgical site at Buriram Province, northeastern Thailand: A view from luminescence dating. Archaeological Research in Asia 31, 100395, http://doi.org/10.1016/j.ara.2022.100395

Lei, H.-R., Zhou, Z.-Y., Guo, Y.-J., Du, J.-H., Zhang, J.-F., 2022. Chronology of the Paleolithic site of Xibaimaying in the Nihewan Basin, North China, inferred from optical dating of fine-grained quartz. Quaternary Geochronology 72, 101363, http://doi.org/10.1016/j.quageo.2022.101363

Moreno, D., Ortega, A.I., Falguères, C., Shao, Q., Tombret, O., Gómez-Olivencia, A., Aranburu, A., Trompier, F., Bermúdez de Castro, J.M., Carbonell, E., Arsuaga, J.L., 2022. ESR/U-series chronology of the Neanderthal occupation layers at Galería de las Estatuas (Sierra de Atapuerca, Spain). Quaternary Geochronology 72, 101342, http://doi.org/10.1016/j.quageo.2022.101342

Nirgi, T., Grudzinska, I., Kalińska, E., Konsa, M., Jõeleht, A., Alexanderson, H., Hang, T., Rosentau, A., 2022. Late-Holocene relative sea-level changes and palaeoenvironment of the Pre-Viking Age ship burials in Salme, Saaremaa Island, eastern Baltic Sea. The Holocene 32, 237-253, http://doi.org/10.1177/09596836211066596

Norman, K., Shipton, C., O'Connor, S., Malanali, W., Collins, P., Wood, R., Saktura, W.M., Roberts, R.G., Jacobs, Z., 2022. Human occupation of the Kimberley coast of northwest Australia 50,000 years ago. Quaternary Science Reviews 288, 107577, http://doi.org/10.1016/j.quascirev.2022.107577

Preoteasa, L., Vespremeanu-Stroe, A., Dan, A., Țuțuianu, L., Panaiotu, C., Stoica, M., Sava, T., Iancu, L.M., Stănică, A.-D., Zăinescu, F., Mirea, D.A., Olteanu, D.C., Pupim, F.N., Ailincăi, S., 2021. Late-Holocene landscape evolution and human presence in the northern Danube delta (Chilia distributary lobes). The Holocene 31, 1459-1475, http://doi.org/10.1177/09596836211019121

Richter, M., Tsukamoto, S., Chapot, M.S., Duller, G.A.T., Barham, L.S., 2022. Electron spin resonance dating of quartz from archaeological sites at Victoria Falls, Zambia. Quaternary Geochronology 72, 101345, http://doi.org/10.1016/j.quageo.2022.101345

Rigot, J.-B., Gondet, S., Chambrade, M.-L., Djamali, M., Mohammadkhani, K., Thamó-Bozsó, E., 2022. Pulvar River changes in the Pasargadae plain (Fars, Iran) during the Holocene and the consequences for water management in the first millennium BCE. Quaternary International 635, 83-104, http://doi.org/10.1016/j.quaint.2021.05.012

Schilt, F., Miller, C.E., Wright, D.K., Mentzer, S.M., Mercader, J., Moss, P., Choi, J.-H., Siljedal, G., Clarke, S., Mwambwiga, A., Thomas, K., Barbieri, A., Kaliba, P., Gomani-Chindebvu, E., Thompson, J.C., 2022. Hunter-gatherer environments at the Late Pleistocene sites of Mwanganda's Village and Bruce, northern Malawi. Quaternary Science Reviews 292, 107638, http://doi.org/10.1016/j.quascirev.2022.107638

Smith, M.F., 2020. Geoarchaeological investigations at the Ryan-Harley Paleoindian site, Florida (8JE1004): Implications for human settlement of the Wacissa River Basin during the Younger Dryas. Geoarchaeology 35, 451-466, http://doi.org/10.1002/gea.21784

Smith, M.F., 2022. Geoarchaeological Excavations at the Guest Mammoth Site (8MR130), Florida, USA. Quaternary Science Reviews 279, 107385, http://doi.org/10.1016/j.quascirev.2022.107385

Srisunthon, P., Mueller, D., Preusser, F., 2022. Decline of Lanna ceramic group production in northern Thailand (Ban Bo Suak site) confined by radiocarbon and luminescence dating. Archaeological and Anthropological Sciences 14, 149, http://doi.org/10.1007/s12520-022-01618-y

Tribolo, C., Mercier, N., Dumottay, C., Cantin, N., Banks, W.E., Stratford, D., de la peña, P., Backwell, L., Wadley, L., Francesco, d.E., 2022. Luminescence dating at Border Cave: attempts, questions, and new results. Quaternary Science Reviews 296, 107787, http://doi.org/10.1016/j.quascirev.2022.107787

Waselkov, G.A., Beebe, D.A., Cyr, H., Chamberlain, E.L., Mehta, J.M., Nelson, E.S., 2022. History and Hydrology: Engineering Canoe Canals in the Estuaries of the Gulf of Mexico. Journal of Field Archaeology 47, 486-500, http://doi.org/10.1080/00934690.2022.2090747

Weiss, M., Hein, M., Urban, B., Stahlschmidt, M.C., Heinrich, S., Hilbert, Y.H., Power, R.C., Suchodoletz, H.v., Terberger, T., Böhner, U., Klimscha, F., Veil, S., Breest, K., Schmidt, J., Colarossi, D., Tucci, M., Frechen, M., Tanner, D.C., Lauer, T., 2022. Neanderthals in changing environments from MIS 5 to early MIS 4 in northern Central Europe – Integrating archaeological, (chrono)stratigraphic and paleoenvironmental evidence at the site of Lichtenberg. Quaternary Science Reviews 284, 107519, http://doi.org/10.1016/j.quascirev.2022.107519

Wiśniewski, A., Jary, Z., Moska, P., Pyżewicz, K., Ciombor, M., Krawczyk, M., Kasprzak, M., 2022. Middle Palaeolithic, Transitional or Upper Palaeolithic: Geoarchaeological revision of the southern part of the loess site Dzierżysław 1, SW Poland. Quaternary International 632, 94-111, http://doi.org/10.1016/j.quaint.2021.10.015

Wroth, K., Tribolo, C., Bousman, C.B., Horwitz, L.K., Rossouw, L., Miller, C.E., Toffolo, M.B., 2022. Human occupation of the semi-arid grasslands of South Africa during MIS 4: New archaeological and paleoecological evidence from Lovedale, Free State. Quaternary Science Reviews 283, 107455, http://doi.org/10.1016/j.quascirev.2022.107455

Zhang, J.-F., Hou, Y.-M., Guo, Y.-J., Rui, X., Wang, Z.-H., Yang, Z.-M., Liu, Y., Zhen, Z.-M., Hu, Y., Zhou, L.-P., 2022. Radiocarbon and luminescence dating of the Wulanmulun site in Ordos, and its implication for the chronology of Paleolithic sites in China. Quaternary Geochronology 72, 101371, http://doi.org/10.1016/j.quageo.2022.101371

ESR, applied in various contexts

Ji, H., Liu, C.-R., Zhang, P.-Q., Wei, C.-Y., Li, B.-S., Yin, G.-M., 2022. The upper dating limit of the ESR signal at g=2.0006 in recrystallized carbonates. Radiation Measurements 157, 106830, http://doi.org/10.1016/j.radmeas.2022.106830

Khan, A.A., Shahid, M.K., 2023. Identification of radiation processing of different plant foods of Pakistan origin using the rapid technique of Electron Spin Resonance (ESR) spectrometry. Radiation Physics and Chemistry 204, 110667, http://doi.org/10.1016/j.radphyschem.2022.110667

Liu, C.-R., Ji, H., Li, W.-P., Wei, C.-Y., Yin, G.-M., 2022. The relationship between irradiation sensitivity of quartz Al and Ti centers and baking temperature by volcanic lava flow: Example of Datong volcanic group, China. Radiation Measurements 157, 106823, http://doi.org/10.1016/j.radmeas.2022.106823

Moreno, D., Ortega, A.I., Falguères, C., Shao, Q., Tombret, O., Gómez-Olivencia, A., Aranburu, A., Trompier, F., Bermúdez de Castro, J.M., Carbonell, E., Arsuaga, J.L., 2022. ESR/U-series chronology of the Neanderthal occupation layers at Galería de las Estatuas (Sierra de Atapuerca, Spain). Quaternary Geochronology 72, 101342, http://doi.org/10.1016/j.quageo.2022.101342

Niu, Y., Fan, Y., Qiao, Y., Lü, T., Li, C., Qi, L., Wang, S., Peng, S., Tan, Y., 2022. Chronostratigraphy of a loess-paleosol sequence in the western Chinese Loess Plateau based on ESR dating and magnetostratigraphy. Quaternary International 637, 1-11, http://doi.org/10.1016/j.quaint.2022.08.005

Oka, T., Takahashi, A., Koarai, K., Kino, Y., Sekine, T., Shimizu, Y., Chiba, M., Suzuki, T., Osaka, K., Sasaki, K., Shinoda, H., 2022. Detection limit of electron spin resonance for Japanese deciduous tooth enamel and density separation method for enamel–dentine separation. Journal of Radiation Research 63, 609-614, http://doi.org/10.1093/jrr/rrac033

Richter, M., Tsukamoto, S., Chapot, M.S., Duller, G.A.T., Barham, L.S., 2022. Electron spin resonance dating of quartz from archaeological sites at Victoria Falls, Zambia. Quaternary Geochronology 72, 101345, http://doi.org/10.1016/j.quageo.2022.101345

Yu, W., Herries, A.I.R., Joannes-Boyau, R., 2022. Using X-rays as an irradiation source for direct ESR dating of fossil teeth. Quaternary Geochronology 72, 101372, http://doi.org/10.1016/j.quageo.2022.101372

Basic research

Ataee, N., Roberts, H.M., Duller, G.A.T., 2022. Isolating a violet stimulated luminescence (VSL) signal in quartz suitable for dating: Investigating different thermal treatments and signal integration limits. Radiation Measurements 156, 106810, http://doi.org/10.1016/j.radmeas.2022.106810

Autzen, M., Andersen, C.E., Bailey, M., Murray, A.S., 2022. Calibration quartz: An update on dose calculations for luminescence dating. Radiation Measurements 157, 106828, http://doi.org/10.1016/j.radmeas.2022.106828

Azorín-Nieto, J., Furetta, C., Ortiz-Martínez, E., Azorin-Vega, C., 2022. Calculation of the half life for the thermoluminescent signal of Beryllium oxide. Applied Radiation and Isotopes 186, 110291, http://doi.org/10.1016/j.apradiso.2022.110291

Bench, T., Feathers, J., 2022. Trialing the application of controlled exposure experiments for optical exposure dating on quartzite quarry surfaces in Washington State. Radiation Measurements 156, 106805, http://doi.org/10.1016/j.radmeas.2022.106805

Biernacka, M., Chruścińska, A., Palczewski, P., Derkowski, P., 2022. Determining the kinetic parameters of traps in quartz using the thermally modulated OSL method. Journal of Luminescence 252, 119289, http://doi.org/10.1016/j.jlumin.2022.119289

Chapot, M.S., Duller, G.A.T., Barham, L.S., 2022. Challenges of dating quartz OSL samples with saturated grains: Lessons from single-grain analyses of low dose-rate samples from Victoria Falls, Zambia. Quaternary Geochronology 72, 101344, http://doi.org/10.1016/j.quageo.2022.101344

Cui, F., Qin, J., Liu, J., Fan, P., Li, Z., Li, K., Chen, J., 2022. Isolating quartz-dominated OSL signal of rock slice by using pulsed stimulation: Implications for dating burial age of cobbles. Quaternary Geochronology 72, 101367, http://doi.org/10.1016/j.quageo.2022.101367

Devi, M., Chauhan, N., Rajapara, H., Joshi, S., Singhvi, A.K., 2022. Multispectral athermal fading rate measurements of K-feldspar. Radiation Measurements 156, 106804, http://doi.org/10.1016/j.radmeas.2022.106804

Fitzgerald, S.K., Sanderson, D.C.W., Cresswell, A.J., Martin, L., 2022. Using Infra-red stimulated luminescence and phototransferred thermoluminescence to investigate electron trapping and charge transport in feldspars. Radiation Measurements 156, 106817, http://doi.org/10.1016/j.radmeas.2022.106817

Ivester, A.H., Rhodes, E.J., Dolan, J.F., Van Dissen, R.J., Gauriau, J., Little, T., McGill, S.F., Tuckett, P.A., 2022. A method to evaluate the degree of bleaching of IRSL signals in feldspar: The 3ET method. Quaternary Geochronology 72, 101346, http://doi.org/10.1016/j.quageo.2022.101346

Ji, H., Liu, C.-R., Zhang, P.-Q., Wei, C.-Y., Li, B.-S., Yin, G.-M., 2022. The upper dating limit of the ESR signal at g=2.0006 in recrystallized carbonates. Radiation Measurements 157, 106830, http://doi.org/10.1016/j.radmeas.2022.106830

Kalita, J.M., Chithambo, M.L., 2020. Structural, compositional and thermoluminescence properties of microcline (KAlSi3O8). Journal of Luminescence 224, 117320, http://doi.org/10.1016/j.jlumin.2020.117320

Kreutzer, S., Mercier, N., Lamothe, M., 2022. Infrared-radiofluorescence: Dose saturation and long-term signal stability of a K-feldspar sample. Radiation Measurements 156, 106818, http://doi.org/10.1016/j.radmeas.2022.106818

Kundu, M., Chakrabarty, S., Bhattacharyya, S., Majumdar, P.S., 2022. Thermoluminescence glow curve analysis using temperature dependent frequency factor in OTOR model. Radiation Measurements 156, 106820, http://doi.org/10.1016/j.radmeas.2022.106820

Liu, C.-R., Ji, H., Li, W.-P., Wei, C.-Y., Yin, G.-M., 2022. The relationship between irradiation sensitivity of quartz Al and Ti centers and baking temperature by volcanic lava flow: Example of Datong volcanic group, China. Radiation Measurements 157, 106823, http://doi.org/10.1016/j.radmeas.2022.106823

Monti, A.M., Ricci, G., Martini, M., Galli, A., Lugli, F., Dalconi, M.C., Artioli, G., 2022. Unusual Luminescence of Quartz from La Sassa, Tuscany: Insights on the Crystal and Defect Nanostructure of Quartz Further Developments. Minerals 12, 828, https://www.mdpi.com/2075-163X/12/7/828

Morthekai, P., Tiwari, P., Murari, M.K., Singh, P., Thakur, B., Manoj, M.C., Ali, S.N., Singh, V.K., Kumar, K., Rai, J., Dubey, N., Srivastava, P., 2022. Further investigations towards luminescence dating of diatoms. Radiation Measurements 156, 106803, http://doi.org/10.1016/j.radmeas.2022.106803

Poolton, N.R.J., Kars, R.H., 2022. On the linewidth of luminescence emission bands in alkali feldspars. Radiation Measurements 158, 106848, http://doi.org/10.1016/j.radmeas.2022.106848

Sholom, S., McKeever, S.W.S., 2022. Observations of optically and thermally stimulated luminescence from aluminosilicate glasses. Journal of Luminescence 252, 119254, http://doi.org/10.1016/j.jlumin.2022.119254

Tariwong, Y., Chanthima, N., Kiwsakunkran, N., Kim, H.J., Rajaramakrishna, R., Kothan, S., Kaewkhao, J., 2022. Radiance properties of corundum and feldspar minerals under X-ray induced luminescence. Radiation Physics and Chemistry 199, 110391, http://doi.org/10.1016/j.radphyschem.2022.110391

Tribolo, C., Mercier, N., Dumottay, C., Cantin, N., Banks, W.E., Stratford, D., de la peña, P., Backwell, L., Wadley, L., Francesco, d.E., 2022. Luminescence dating at Border Cave: attempts, questions, and new results. Quaternary Science Reviews 296, 107787, http://doi.org/10.1016/j.quascirev.2022.107787

Yu, W., Herries, A.I.R., Joannes-Boyau, R., 2022. Using X-rays as an irradiation source for direct ESR dating of fossil teeth. Quaternary Geochronology 72, 101372, http://doi.org/10.1016/j.quageo.2022.101372

Zhang, J., Tsukamoto, S., 2022. A simplified multiple aliquot regenerative dose protocol to extend the dating limit of K-feldspar pIRIR signal. Radiation Measurements 157, 106827, http://doi.org/10.1016/j.radmeas.2022.106827

Beyond quartz and K-feldspar: non-traditional minerals

- carbonates

Ji, H., Liu, C.-R., Zhang, P.-Q., Wei, C.-Y., Li, B.-S., Yin, G.-M., 2022. The upper dating limit of the ESR signal at g=2.0006 in recrystallized carbonates. Radiation Measurements 157, 106830, http://doi.org/10.1016/j.radmeas.2022.106830

- diatom

Morthekai, P., Tiwari, P., Murari, M.K., Singh, P., Thakur, B., Manoj, M.C., Ali, S.N., Singh, V.K., Kumar, K., Rai, J., Dubey, N., Srivastava, P., 2022. Further investigations towards luminescence dating of diatoms. Radiation Measurements 156, 106803, http://doi.org/10.1016/j.radmeas.2022.106803

Dose rate interests

Cunningham, A.C., Buylaert, J.-P., Murray, A.S., 2022. Attenuation of beta radiation in granular matrices: implications for trapped-charge dating. Geochronology 4, 517-531, http://doi.org/10.5194/gchron-4-517-2022

Ou, X.J., Roberts, H.M., Duller, G.A.T., 2022. Rapid assessment of beta dose variation inside cobbles, and implications for rock luminescence dating. Quaternary Geochronology 72, 101349, http://doi.org/10.1016/j.quageo.2022.101349

Dosimetry

Azorín-Nieto, J., Furetta, C., Ortiz-Martínez, E., Azorin-Vega, C., 2022. Calculation of the half life for the thermoluminescent signal of Beryllium oxide. Applied Radiation and Isotopes 186, 110291, http://doi.org/10.1016/j.apradiso.2022.110291

Kara, E., Hicsonmez, A., 2022. Physical and dosimetric characteristic properties of BeO OSL for clinical dosimetric measurements. Applied Radiation and Isotopes 186, 110199, http://doi.org/10.1016/j.apradiso.2022.110199

Khan, A.A., Shahid, M.K., 2023. Identification of radiation processing of different plant foods of Pakistan origin using the rapid technique of Electron Spin Resonance (ESR) spectrometry. Radiation Physics and Chemistry 204, 110667, http://doi.org/10.1016/j.radphyschem.2022.110667

Khandaker, M.U., Nawi, S.N.M., Lam, S.E., Bradley, D.A., Sani, S.F.A., Faruque, M.R.I., Yasmin, S., Idris, A.M., 2022. Studies of defect states and kinetic parameters of car windscreen for thermoluminescence retrospective dosimetry. Applied Radiation and Isotopes 186, 110271, http://doi.org/10.1016/j.apradiso.2022.110271

Oka, T., Takahashi, A., Koarai, K., Kino, Y., Sekine, T., Shimizu, Y., Chiba, M., Suzuki, T., Osaka, K., Sasaki, K., Shinoda, H., 2022. Detection limit of electron spin resonance for Japanese deciduous tooth enamel and density separation method for enamel–dentine separation. Journal of Radiation Research 63, 609-614, http://doi.org/10.1093/jrr/rrac033

Yukihara, E.G., Bos, A.J.J., Bilski, P., McKeever, S.W.S., 2022. The quest for new thermoluminescence and optically stimulated luminescence materials: Needs, strategies and pitfalls. Radiation Measurements 158, 106846, http://doi.org/10.1016/j.radmeas.2022.106846

Instruments

Sohbati, R., Kook, M., Jain, M., Thomsen, K.J., Murray, A.S., 2023. Development of a wide-field EMCCD camera-based alpha-particle imaging system. Measurement 206, 112234, http://doi.org/10.1016/j.measurement.2022.112234

Portable instruments

Adolph, M.-L., Lampe, R., Lorenz, S., Haberzettl, T., 2022. Characterization of (paleo)lacustrine landforms using sedimentological and portable OSL investigations at Schweriner See, north-eastern Germany. Earth Surface Processes and Landforms 47, 422-435, http://doi.org/10.1002/esp.5258

Janovský, M.P., Horák, J., Ackermann, O., Tavger, A., Cassuto, D., Šmejda, L., Hejcman, M., Anker, Y., Shai, I., 2022. The contribution of POSL and PXRF to the discussion on sedimentary and site formation processes in archaeological contexts of the southern Levant and the interpretation of biblical strata at Tel Burna. Quaternary International 618, 24-34, http://doi.org/10.1016/j.quaint.2020.11.045

Robins, L., Roskin, J., Yu, L., Bookman, R., Greenbaum, N., 2022. Aeolian-fluvial processes control landscape evolution along dunefield margins of the northwestern Negev (Israel) since the late Quaternary. Quaternary Science Reviews 285, 107520, http://doi.org/10.1016/j.quascirev.2022.107520

Laboratory protocols (De, sample preparation)

Singh, A.K., Manna, I., Kumar, P., Dawar, A., Kumar, P., Murari, M.K., 2022. A new and effective method for quartz-feldspar separation for OSL and CRN dating. Quaternary Geochronology 72, 101315, http://doi.org/10.1016/j.quageo.2022.101315

Woor, S., Durcan, J.A., Burrough, S.L., Parton, A., Thomas, D.S.G., 2022. Evaluating the effectiveness of heavy liquid density separation in isolating K-feldspar grains using alluvial sediments from the Hajar Mountains, Oman. Quaternary Geochronology 72, 101368, http://doi.org/10.1016/j.quageo.2022.101368

Review

Yukihara, E.G., Bos, A.J.J., Bilski, P., McKeever, S.W.S., 2022. The quest for new thermoluminescence and optically stimulated luminescence materials: Needs, strategies and pitfalls. Radiation Measurements 158, 106846, http://doi.org/10.1016/j.radmeas.2022.106846

Book, for the interest for all

While the publication below does not deal with luminescence or ESR dating, we believe the subject matter is of interest to all of us. Moreover, this collection of essays was edited by a member of the luminescence community

Singhvi, A.K., 2022. Essays on social responsibility of scientists: preface. Proceedings of the Indian National Science Academy 88, 812-814, http://doi.org/10.1007/s43538-022-00123-z

Conference Announcements: 14th International Conference "Methods of Absolute Chronology"

Dear Colleagues,

With a year's delay due to the pandemic, we are back in physical form!

The Gliwice Absolute DAting Methods Centre, Institute of Physics – Centre for Science and Education at the Silesian University of Technology would like to invite you to take part in the 14th International Conference "Methods of Absolute Chronology", which will be held from 17th to 19th May, 2023 in Gliwice, Poland.

We are striving at providing a platform of exchange in the area of quaternary dating methods and their applications. We are looking forward to receiving submissions that will cover a range of subjects to foster an exchange of ideas.

The conference scientific programme includes plenary and poster sessions. The working language of the conference is English. Any questions related to the conference can be directed to the e-mail address: mach2023@polsl.pl.

Please register and submit your abstract on the website (https://mach2023.polsl.pl/ and indicate preferred session and presentation form (oral/poster). The accepted presentations will be published in the open-access journal "Geochronometria",–following the regular reviewing schedule. We have secured funding to waive a fee for selected manuscripts.

AREAS COVERED

Depending on the scope of received abstracts the following list may be updated by the Scientific Committee:

Terrestrial archives	*Applications in geosciences*
Advances in luminescence dating	*Diet/stable isotopes*
Geoarchaeology	*Advances in radiocarbon dating*
Mortars	*Applications in archaeology*
Anthropocene/anthropogenic impact	*Bio-components/biofuel*

IMPORTANT DATES

Registration starts: **19 December 2022**
Submission of abstracts and registration: **11 March 2023**
Abstract acceptance: **31 March 2023**
Payment: **10 April 2023**
Second circular: **31 March 2023**
Conference: **17-19 May 2023**
Submission of manuscripts: **30 June 2023**

On behalf of the Local Organising Committee
Piotr Moska and Grzegorz Adamiec

Conference Announcements: German LED 2023

Save the Date:

German LED meeting
9th – 11th November 2023
Innsbruck
Austria

Details will be announced here in February 2023:
https://quaternary.uibk.ac.at/Research/Current-Research/Luminescence-geochronology.aspx

Any requests for joining the e-mail distribution list please direct to: Michael.Meyer@uibk.ac.at

Best wishes,
Michael Meyer

Ancient TL
ISSN 2693-0935

Aims and Scope
Ancient TL is a journal devoted to Luminescence dating, Electron Spin Resonance (ESR) dating, and related techniques. It aims to publish papers dealing with experimental and theoretical results in this field, with a minimum of delay between submission and publication. Ancient TL also publishes a current bibliography, thesis abstracts, letters, and miscellaneous information, e.g., announcements for meetings.

Frequency
Two issues per annum in June and December

Submission of articles to Ancient TL
Ancient TL has a reviewing system in which direct dialogue is encouraged between reviewers and authors. For instructions to authors and information on how to submit to Ancient TL, please visit the website at:
http://ancienttl.org/TOC1.htm

Journal Enquiries
For enquiries please contact the editor:
Regina DeWitt, Department of Physics, East Carolina University, Howell Science Complex, 1000 E. 5th Street, Greenville, NC 27858, USA; Tel: +252-328-4980; Fax: +252-328-0753 (dewittr@ecu.edu)

Subscriptions to Ancient TL
Ancient TL Vol. 32 No.2 December 2014 was the last issue to be published in print. Past and current issues are available for download free of charge from the Ancient TL website:
http://ancienttl.org/TOC4.htm